

Directional Neutron Detector Project

*Coated Gallium Arsenide Neutron Detectors:
Results of Characterization Measurements*

Nuclear Engineering Division

About Argonne National Laboratory

Argonne is a U.S. Department of Energy laboratory managed by The University of Chicago under contract W-31-109-Eng-38. The Laboratory's main facility is outside Chicago, at 9700 South Cass Avenue, Argonne, Illinois 60439. For information about Argonne, see www.anl.gov.

Availability of This Report

This report is available, at no cost, at <http://www.osti.gov/bridge>. It is also available on paper to the U.S. Department of Energy and its contractors, for a processing fee, from:

U.S. Department of Energy

Office of Scientific and Technical Information

P.O. Box 62

Oak Ridge, TN 37831-0062

phone (865) 576-8401

fax (865) 576-5728

reports@adonis.osti.gov

Disclaimer

This report was prepared as an account of work sponsored by an agency of the United States Government. Neither the United States Government nor any agency thereof, nor The University of Chicago, nor any of their employees or officers, makes any warranty, express or implied, or assumes any legal liability or responsibility for the accuracy, completeness, or usefulness of any information, apparatus, product, or process disclosed, or represents that its use would not infringe privately owned rights. Reference herein to any specific commercial product, process, or service by trade name, trademark, manufacturer, or otherwise, does not necessarily constitute or imply its endorsement, recommendation, or favoring by the United States Government or any agency thereof. The views and opinions of document authors expressed herein do not necessarily state or reflect those of the United States Government or any agency thereof, Argonne National Laboratory, or The University of Chicago.

Directional Neutron Detector Project

Coated Gallium Arsenide Neutron Detectors: Results of Characterization Measurements

by
R.T. Klann, G. Perret, J. Sanders
Nuclear Engineering Division, Argonne National Laboratory

March 31, 2006

work sponsored by
Department of Homeland Security
Science And Technology Directorate
Office of Research and Development
Radiological and Nuclear Countermeasures Program

Abstract

Effective detection of special nuclear materials (SNM) is essential for reducing the threat associated with stolen or improvised nuclear devices. Passive radiation detection technologies are primarily based on gamma-ray detection and subsequent isotope identification or neutron detection (specific to neutron sources and SNM).

One major effort supported by the Department of Homeland Security in the area of advanced passive detection is handheld or portable neutron detectors for search and localization tasks in emergency response and interdiction settings. A successful SNM search detector will not only be able to confirm the presence of fissionable materials but also establish the location of the source in as short of time as possible while trying to minimize false alarms due to varying background or naturally occurring radioactive materials (NORM). For instruments based on neutron detectors, this translates to detecting neutrons from spontaneous fission or alpha-n reactions and being able to determine the direction of the source (or localizing the source through subsequent measurements).

Polyethylene-coated gallium arsenide detectors were studied because the detection scheme is based on measuring the signal in the gallium arsenide wafers from the electrical charge of the recoil protons produced from the scattering of neutrons from the hydrogen nucleus. The inherent reaction has a directional dependence because the neutron and hydrogen nucleus have equivalent masses.

The assessment and measurement of polyethylene-coated gallium arsenide detector properties and characteristics was the first phase of a project being performed for the Department of Homeland Security and the results of these tests are reported in this report. The ultimate goal of the project was to develop a man-portable neutron detection system that has the ability to determine the direction of the source from the detector.

The efficiency of GaAs detectors for different sizes of polyethylene layers and different angles between the detector and the neutron source were determined. Preliminary measurements with a neutron generator based on a deuterium-tritium reaction (~14 MeV neutrons) were performed and the results are discussed. This report presents the results of these measurements in terms of efficiency and angular efficiency and compares them to Monte Carlo calculations to validate the calculation scheme in view of further applications.

Based on the results of this study, the polyethylene-coated gallium arsenide detectors provide adequate angular resolution based on proton recoil detection from the neutron scattering reaction from hydrogen. However, the intrinsic efficiency for an individual detector is extremely low. Because of this low efficiency, large surface area detectors (or a large total surface area from many small detectors) would be required to generate adequate statistics to perform directional detection in near-real time. Large surface areas could be created by stacking the detector wafers with only a negligible attenuation of source neutrons. However, the cost of creating such a large array of GaAs is cost-prohibitive at this time.

Table of Contents

Abstract	i
1. Introduction.....	1
2. Background.....	2
2.1. Neutron Detection Principles.....	2
2.2. Detection Methods.....	4
3. Experiments.....	6
3.1. Source Strength Measurements.....	9
3.2. Measurements with Lead and Cadmium Sheets.....	10
3.3. Background Measurements.....	11
3.4. Effect of the High Voltage.....	11
3.5. Efficiency.....	15
3.6. Angular Response.....	17
4. Calculations.....	20
5. Comparisons.....	22
5.1. Efficiency.....	22
5.2. Angular Response.....	23
6. Conclusions.....	28
References.....	30
Appendix 1: Argonne National Laboratory Intra-Laboratory Memorandum on the Output of the MF-Physics A-711 Neutron Generator.....	31

List of Figures

Figure 1: Watt Fission Source Distribution from Spontaneous Fission of Cf-252.....	4
Figure 2: Neutron Capture Cross-Section for Cd-113	5
Figure 3: Polyethylene coated gallium arsenide detector	7
Figure 4: Scheme of the acquisition chain.....	7
Figure 5: Scheme of the experimental layout	9
Figure 6: Pulse height spectra with and without lead and cadmium sheet	10
Figure 7: Background measurement	11
Figure 8: Pulse height spectra of the 1cm ² square, 80 mils thick detector at different high voltages	13
Figure 9: Pulse height spectra of the 1 cm ² square, 10 mils thick, detector for different high voltages	13
Figure 10: Example of gaussian fit of the pulse height spectra	14
Figure 11: Pulse height spectra as a function of the CH ₂ thickness.....	16
Figure 12: Measured absolute efficiency for different CH ₂ thickness.....	16
Figure 13: Pulse height spectra as a function of the detector angle with the neutron source beam.....	17
Figure 14: Measured angular response	18
Figure 15: Normalized angular response with background subtraction	20
Figure 16: ENDFB6.8 cross sections for natural carbon	21
Figure 17: ENDFB6.8 elastic scattering cross section for hydrogen.....	21
Figure 18: Intrinsic efficiency of the 0.25 cm ² round and 1 cm ² square detectors.....	23
Figure 19: Measured and calculated normalized efficiency of the 80 mils thick CH ₂ layer detector.....	24
Figure 20: Measured and calculated normalized efficiency of the 10 mils thick CH ₂ layer detector.....	25
Figure 21: Measured and calculated normalized efficiency of the 2 mils thick CH ₂ layer detector.....	25
Figure 22: Measured and calculated absolute angular efficiency of the 80 mils CH ₂ thick detector.....	27
Figure 23: Measured and calculated absolute angular efficiency of the 2 and 10 mils CH ₂ thick detectors	27

List of Tables

Table 1: Measured Prompt Fission Multiplicity Distributions	3
Table 2: List of Measurements	8
Table 3: Neutron Source Strength.....	9
Table 4: Relationship Between the High Voltage and the Voltage on the Gold Contact.....	12
Table 5: Integrated Count Rates for Different High Voltages.....	14
Table 6: Measured Intrinsic Efficiency per Surface Unit.....	15
Table 7: Measured Angular Response	18
Table 8: Measured Intrinsic Efficiency.....	22
Table 9: Normalized Response due to Proton Interaction in the GaAs – 80 mils CH ₂ Detector.....	24
Table 10: Normalized Response due to Proton Interaction in the GaAs – 2 and 10 mils CH ₂ Detector.....	24
Table 11: Intrinsic Efficiency per Unit Area – 80 mils CH ₂ Detector.....	26
Table 12: Intrinsic Efficiency per Unit Area – 2 and 10 mils CH ₂ Detector	26

Introduction

The Department of Homeland Security (DHS) is committed to using cutting edge technologies and scientific talent in the quest to make America safer. The Science & Technology (S&T) directorate of DHS is tasked with researching and organizing the scientific, engineering and technological resources of the United States and leveraging these existing resources into technological tools to help protect the homeland. The Radiological and Nuclear (RAD/NUC) Countermeasures Portfolio supports this effort for detecting Special Nuclear Materials (SNM) through the Passive Detection Thrust Area.

Passive radiation detection technologies are key to detecting and characterizing nuclear emissions in a wide range of applications. Existing technologies provide a valuable first level of defense that can be considerably extended by focused technology development. The overall goal of the program is to develop new capabilities in the radiation detection area and then transfer these technologies to commercial entities so that the technologies can be effectively transferred to the private sector.

The passive detection program is broad-based with efforts in a number of key areas. These areas include: the development of gamma-ray and neutron detectors, imagers, and directional detectors, and improved algorithms. Particular focus is placed on technologies that provide an increase in the effective sensitivity and specificity (improved ability to detect sources in the midst of distributed backgrounds and nuisance sources), since this is the basis for approaches that increase the probability of detection without increasing the probability of false alarms.

Effective detection of special nuclear materials (SNM) is essential for reducing the threat associated with stolen or improvised nuclear devices. Passive radiation detection technologies are primarily based on gamma-ray detection and subsequent isotope identification or neutron detection (specific to neutron sources and SNM).

One major effort in the area of advanced passive detection is handheld or portable neutron detectors for search and localization tasks in emergency response and interdiction settings. A successful SNM search detector will not only be able to confirm the presence of fissionable materials but also establish the location of the source in as short of time as possible while trying to minimize false alarms due to varying background or naturally occurring radioactive materials (NORM). For instruments based on neutron detectors, this translates to detecting neutrons from spontaneous fission or alpha-n reactions and being able to determine the direction of the source (or localizing the source through subsequent measurements).

The goal of this project is to develop a man-portable neutron detection system that has the ability to determine the direction of the source from the detector. In this manner, it is meant to reduce the time it takes to find and locate a neutron source during search operations.

Because of their high intrinsic efficiency, typical neutron detectors employed today are designed to detect thermal neutrons. Thermal neutrons are the result of scattering of source neutrons from materials present in the environment or near the detector to moderate the neutron energy down to

thermal energies. Because of the multiple scattering involved in these moderating reactions, the angular direction of the original neutron emission cannot be determined.

To detect the direction of the neutron source, the detector should be able to determine or infer the direction of the neutron that is detected. To do this, the detector should detect the uncollided fast neutron resulting from a fission event.

Polyethylene coated gallium arsenide detectors appear to be a good candidate because the detection scheme is based on measuring the signal in the gallium arsenide wafers from the electrical charge of the recoil protons produced from the scattering of neutrons from the hydrogen nucleus. The inherent reaction has a directional dependence because the neutron and hydrogen nucleus have equivalent masses.

Polyethylene-coated gallium arsenide neutron detectors have been produced and tested under previous projects for different applications. However, the directional response of the detectors and other characteristics have never been adequately assessed or measured. The assessment and measurement of the detector properties and characteristics is the first phase of this project and the results of these tests are reported in this report.

The first step is to determine the absolute efficiency of such detectors for different sizes of polyethylene layers and different angles between the detector and the neutron source. Preliminary measurements with a neutron generator based on a deuterium-tritium reaction (~14 MeV neutrons) were performed and the results are discussed here. This report presents the results of these measurements in terms of efficiency and angular efficiency and compares them to Monte Carlo calculations to validate the calculation scheme in view of further applications.

2. Background

In order to improve existing neutron detectors and search operations involving neutron detectors, one must first understand the principles of detection for neutrons. A brief summary of detection principles, including energy spectra, detection reactions, types of detectors, and detection efficiency, is provided.

2.1 Neutron Detection Principles

A neutron is a neutral particle and, by definition, has a net electrical charge of zero similar to a gamma ray. Being uncharged, a neutron does not interact with matter via the Coulomb force like a charged particle. Instead, for a neutron to lose energy and/or be detected, the neutron must interact with the nucleus of an atom.

There are several mechanisms that allow a neutron to interact with the nucleus of an atom and lose energy. When passing through matter, a neutron can scatter from the nucleus of an atom. If the scattering is defined by kinematics, it is referred to as elastic scattering and the momentum and kinetic energy of the particles is conserved in the reaction. If the kinetic energy of the particles is not conserved, then it is referred to as inelastic scattering. In this type of scattering reaction, the nucleus absorbs some of the kinetic energy internally and is left in an excited state.

Neutrons can also be captured or absorbed by a nucleus. These reactions lead to a change in the atomic mass number and/or atomic number of the nucleus. The resulting nucleus, left in an excited state, will then decay to a more stable state. This decay leads to the emission of particles or gamma radiation from the nucleus. These emissions are used to identify the reactions – i.e. (n,p), (n,2n), (n, α), (n, γ), (n,n'), etc. These reactions are listed in shorthand notation; (n,p) means that a nucleus absorbs a neutron and the new nucleus then decays by proton emission. This reaction would reduce the atomic number of the nucleus by one but the atomic mass number (the number of nucleons making up the nucleus) would remain the same.

One special type of neutron absorption reaction results in the fragmentation of the nucleus into two smaller pieces with the emission of additional neutrons. This reaction is known as nuclear fission and can result in the release of any number of neutrons from 1 to 8. These reactions occur only in the elements with the highest atomic mass numbers (90 and higher) – elements known as the actinides or fissionable materials.

Fissionable materials, like uranium and plutonium, are used as the key ingredient to produce nuclear weapons. These materials give the device their enormous explosive yield because of the amount of energy released during the fission process. Fissionable materials are also naturally radioactive and therefore unstable. Unstable nuclei decay by emitting radiation. Fissionable materials will also spontaneously fission, releasing neutrons that can be detected with passive neutron detectors.

A spontaneous fission event, like an induced fission event, releases any number of neutrons from 1 to 8. Table 1 shows the multiplicity of neutron emissions for specific actinide isotopes from spontaneous and induced fission events (ref. 1). The most probable number of neutrons for a fission event is between 1 and 4, and hence the average number of neutrons per fission event is usually between 2 and 3.

Number of Neutrons	Probability Distributions					
	²³⁵ U Induced Fission	²³⁸ Pu Spont. Fission	²³⁹ Pu Induced Fission	²⁴⁰ Pu Spont. Fission	²⁴² Pu Spont. Fission	²⁵² Cf Spont. Fission
0	0.033	0.054	0.011	0.066	0.068	0.002
1	0.174	0.205	0.101	0.232	0.230	0.026
2	0.335	0.380	0.275	0.329	0.334	0.127
3	0.303	0.225	0.324	0.251	0.247	0.273
4	0.123	0.108	0.199	0.102	0.099	0.304
5	0.028	0.028	0.083	0.018	0.018	0.185
6	0.003	-	0.008	0.002	0.003	0.066
7	-	-	-	-	-	0.015
8	-	-	-	-	-	0.002
$\bar{\nu}$	2.406	2.21	2.879	2.156	2.145	3.757

$\bar{\nu}$ is the average number of prompt neutrons per fission event

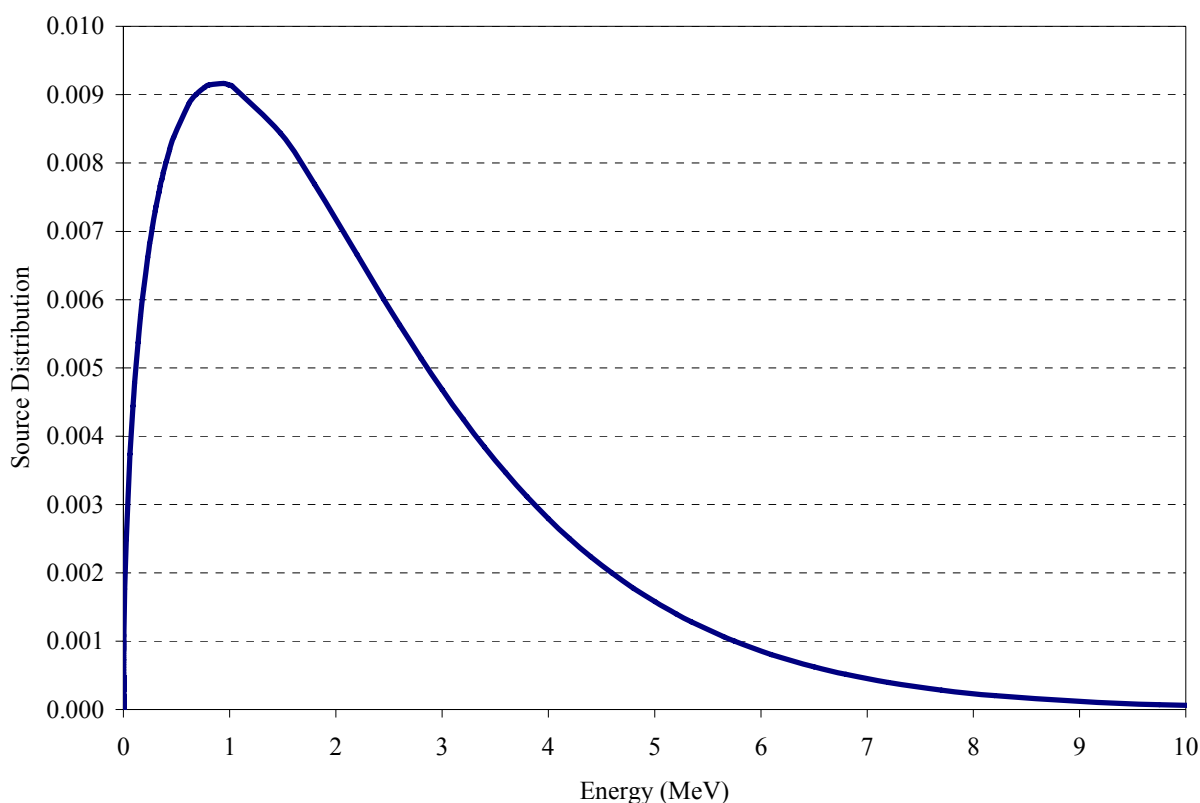


Figure 1: Watt Fission Source Distribution from Spontaneous Fission of ^{252}Cf

Neutrons that are born from fission events are created with a range of energies up to about 10 MeV. The distribution of neutron energies, also known as the neutron spectrum, is shown in Figure 1 for ^{252}Cf . The energy distribution of the emitted neutrons is very similar for other isotopes. The shape of spectrum follows that defined by a Watt fission spectrum (ref. 2). The function of a Watt fission spectrum distribution is given as:

$$f(E) = Ce^{(-E/a)} \sinh(bE)^{1/2}$$

where a and b are constants for a given isotope. The energy spectrum is peaked around 1 MeV (53% of the spectrum is between 0.5 MeV and 2 MeV). There is still a significant fraction of neutrons with energies greater than 2 MeV (42% of the total spectrum is above 2 MeV).

2.2 Detection Methods

The detection of neutrons is based on the neutron interacting with the nuclei in the detector volume and then the resultant charge of the reaction products is deposited in the detector volume. The charge is collected and/or converted to a signal which is then recorded via several different methods. There are numerous specific nuclear reactions that can be used to detect neutrons.

Neutron reaction probability is also called the neutron cross-section. The neutron cross-section is a means to measure and compare the reaction probabilities for different reactions and different

materials. On the macroscopic level, the neutron cross-section is the probability per path length that a reaction will occur, and is given in units of inverse length.

The microscopic cross-section is the probability of reaction with an individual nucleus for a given reaction type for a specific isotope of a material. The microscopic cross-section has units of area and is typically given in barns (10^{-24} cm²/atom). If the microscopic cross-section (σ) is multiplied by the number of nuclei per unit volume (N , in atoms/cm³) then the resultant product is the macroscopic cross-section (Σ).

The probability of reaction for a given reaction is highly dependent upon the energy of the neutron. The probability is a complicated function of neutron energy, but in general, the probability of reaction increases as the neutron energy decreases. An example for the capture cross-section of ¹¹³Cd is shown in Figure 2. One can observe that the cross-section at thermal neutron energies (typically less than 0.5 eV) is orders of magnitude higher than the cross-section at 1 MeV (the peak neutron energy from the ²⁵²Cf spectrum shown in Figure 1).

Because cross-sections around 1 MeV are typically so much lower than cross-sections at thermal neutron energies, most detection schemes rely on slowing down the neutrons. Elastic scattering is the most important process for slowing down neutrons. Materials, known as moderators, are placed around or near the detector volume. Neutrons will then scatter off of the nuclei in the moderator material and lose energy during the scattering process.

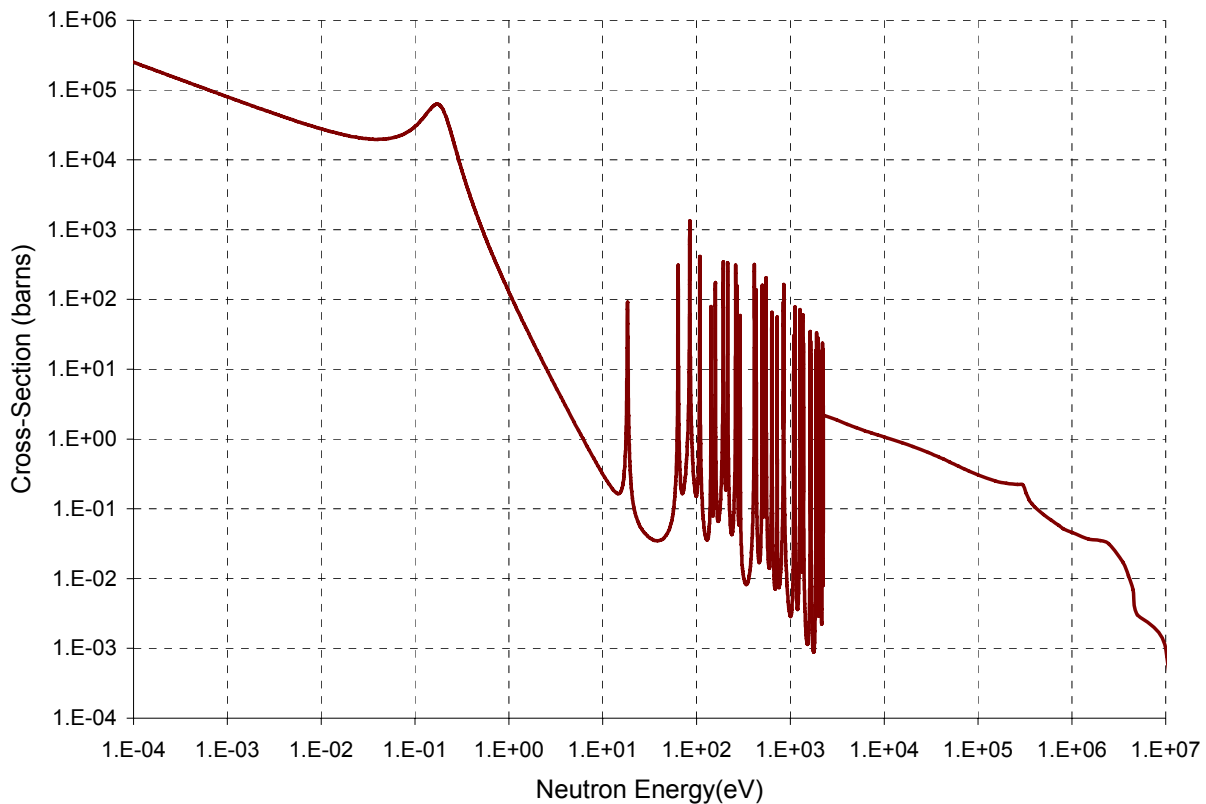


Figure 2: Neutron Capture Cross-Section for ¹¹³Cd

For elastic scattering, the maximum amount of energy that a neutron can transfer to the nucleus in a single collision is

$$Q_{\max} = \frac{4mME}{(M + m)^2},$$

where E is the mass of the neutron, E is the kinetic energy of the neutron, and m is the mass of the nucleus. Hydrogen is the most effective moderator material because a neutron can lose all kinetic energy in a single collision and the average energy loss per collision is one half of the total kinetic energy. The most common moderator material that is used is polyethylene because of the high hydrogen content and density of material. Some detector systems rely on proximity to the human body for moderation because of the large fraction of water in the body.

Not all detectors rely on moderating the neutrons to thermal energies before detection. There are some useful reactions that are utilized at higher neutron energies. One of the potential drawbacks to moderating the neutrons is that the initial energy and direction of the neutron is lost as soon as it scatters from another nucleus. If an uncollided neutron interacts in the detector volume, and the detector has the ability to determine the energy and angle of the neutron, then the source of the neutron can be determined.

The drawback to fast neutron detection is that the relative efficiency compared to thermal neutron reactions is so small that large detector volumes are necessary to obtain comparable efficiencies for interactions in the detector. However, because the fast neutron has not collided and the inherent directional information to the neutron source can be recovered during the detection process, it still makes directional fast neutron detection an attractive alternative.

3. Experiments

Polyethylene-coated gallium arsenide neutron detectors appear to offer this attractive alternative for directional fast neutron detection. The detection scheme is based on the recoil protons from from the scattering of neutrons from the hydrogen nucleus so it has an inherent directional dependence. In addition, GaAs neutron detectors offer the ability to discriminate nuisance signals and can be used for very low counting statistic applications.

A measurement campaign was conducted at the INL NRAD Reactor Facility using an MF-Physics A-711 neutron generator. The neutron generator produces 14 MeV neutrons by deuterium-tritium fusion reaction. The deuteron accelerator is generally operated with an intensity of 2.5 mA and a voltage of 150 kV, with an approximate output of 10^{10} neutrons per second (see section 3.2).

During the measurements, the neutron source strength was monitored by a ^3He detector surrounded by polyethylene to moderate the 14 MeV neutrons. The studied detectors were positioned at 21 or 41 cm away from the neutron generator and were manually rotated to determine the angular response.

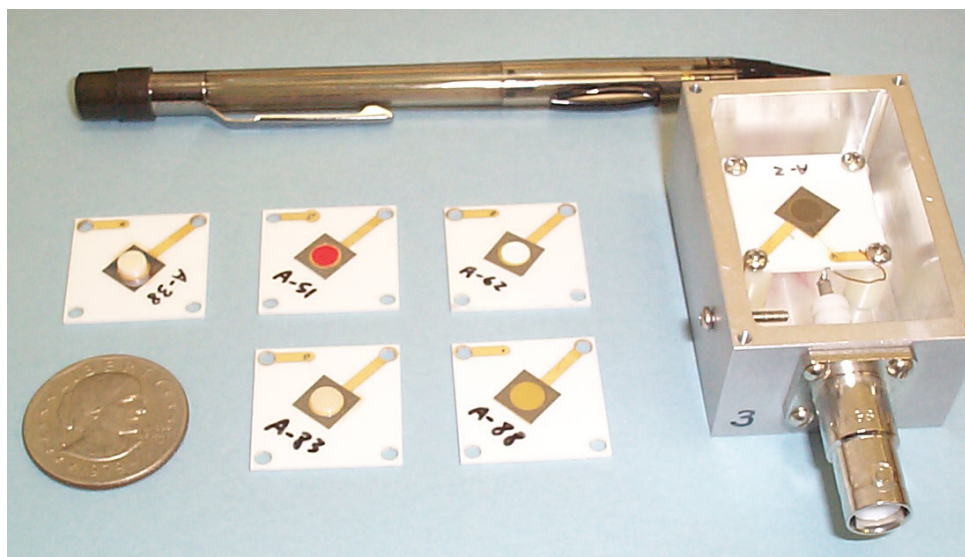


Figure 3: Polyethylene coated gallium arsenide detector

The polyethylene coated gallium arsenide detectors are composed of a layer of polyethylene (CH_2), a gold contact, a layer of gallium arsenide (GaAs) and a second gold contact. The detector is mounted on an alumina backing inside of an aluminum detector box. The detector cross sectional area is either round or square with a 1 cm^2 and a 0.25 cm^2 area. The investigated thicknesses of CH_2 are 2, 5, 10, 35 and 80 mils¹. The gold contact is approximately $1 \mu\text{m}$ thick and the GaAs is $250 \mu\text{m}$ thick. A polyethylene coated GaAs detector is shown in Figure 3.

The acquisition chain was composed of an ORTEC 142 preamplifier whose resistance was changed to $11\text{M}\Omega$, an ORTEC 572 amplifier, an ORTEC Micro-Nomad Multi Channel Analyzer, and a laptop running the Maestro software. The detectors were negatively biased with a high voltage to create an “active” region within the GaAs for charge collection. The thickness of the active region is a function of the negative bias voltage. The bias voltage used varied from 40 to 300V, but the experiments were mainly performed at 60V and 90V. The reported bias voltage is the voltage applied on the power supply. This varies from the actual bias voltage applied to the detection due to losses and resistance in the circuit. Measurements were performed to relate the two values for several detectors. A schematic of the acquisition chain is shown in Figure 4.

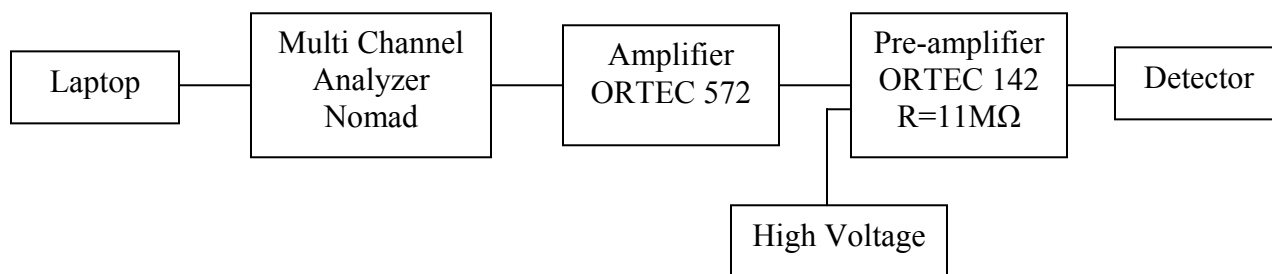


Figure 4: Schematic of the acquisition chain

¹ 1 mil equals $25.4 \mu\text{m}$

The goal of the experiments is to determine the efficiency of detectors as a function of polyethylene thickness and to determine the efficiency of the detectors as a function of angle normal to the neutron source.

Measurements were conducted to establish the neutron generator source strength. In addition, tests were conducted to demonstrate that background levels and detectors response to unwanted radiations (i.e. X ray and gamma ray response) and extracamerall effects were negligible.

The measurements performed are grouped in series and listed in Table 2. The “Lead/Cadmium” series was run to ensure that the X rays and the thermal neutron contribution were negligible, and the “Bias Voltages” series were run to determine the effect of the bias voltage on the charge collection. The efficiency of detectors with different CH₂ thickness was studied in the “Efficiency” series and the angular response was determined in the “Angular” series. A scheme of the experimental layout is shown in Figure 5.

Series Name	Generator	Distance (cm)	Detector cross section	CH ₂ thickness (mils)	Angle (degree)	High Voltage
Lead, Cadmium	150kV 2.5 mA	21	1cm ² square	80	0	60
Bias Voltage 1	150kV 2.5 mA	21	1cm ² square	80	0	50, 60, 70, 80, 90, 100, 110, 130, 150
Bias Voltage 2	150kV 2.5 mA	21	1cm ² square	10	0	60, 90, 120, 150
Angular 1	150kV 2.5 mA	21	1cm ² square	80	0, 30, 60, 90, 120, 150, 180	60
Angular 2	150kV 2.5 mA	21	1cm ² square	80	0, 30, 45, 90, 120, 150, 180	90
Angular 3	150kV 2.5 mA	41	1cm ² square	80	0, 30, 45, 60, 90, 120, 150, 180	90
Angular 4	150kV 2.5 mA	41	1cm ² square	10	0, 30, 45, 60, 90, 120, 180	90
Angular 5	150kV 2.5 mA	21	1cm ² square	2	0, 30, 45, 90, 120, 150, 180	90
Efficiency 1	150kV 2.5 mA	41	1cm ² square	2, 5, 10, 80	0	90
Efficiency 2	150kV 2.5 mA	21	0.25cm ² square	2, 5, 10, 35, 80, bare	0	60

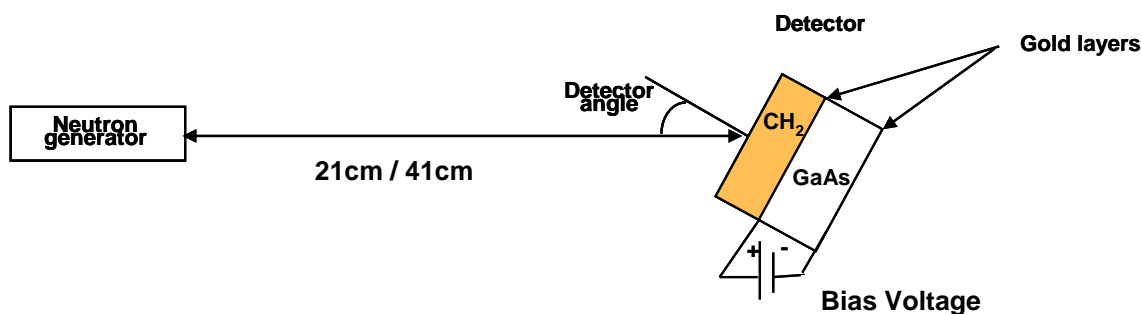


Figure 5: Schematic of the experimental layout

3.1 Source Strength Measurements

The absolute efficiency of a detector is determined by measuring the count rate of the detector (above a certain threshold) and the neutron source strength. In practice, the source strength is measured previously by reaction rates on foils and related to a ^3He tube count rate. The ^3He detector remains in place during the detector measurement and is used to normalize the measurements to the same neutron source strength

Measurements of the source strength are reported in appendix 1 and Table 3. The (n, α) reaction on the aluminum foils is very precise (<1%) but the other measurements disagree at two standard deviations. To account for the disagreement, the uncertainty on the mean source strength is computed as a dispersion on all measurements (without pondering by their uncertainties) and is certainly overestimated.

Unfortunately, the ^3He tube was not active during the source strength measurement and the source strength during the detector measurements cannot be known precisely. Even with the same control settings on the neutron generator, the output can vary by as much as 10% as observed during the measurements. The ^3He tube was active for the detector measurements allowing measurements to be normalized to the same neutron source strength level. The error on the source strength is unknown but can easily be 10% or higher.

Foils	Source (10^{10} n/s)
Ni-58 (n,2n)	0.999 ± 0.024
Ni-58 (n,p)	0.882 ± 0.164
Al-27 (n, α)	1.123 ± 0.006
Fe-56 (n,p)	1.002 ± 0.021
Mean	1.109 ± 0.099

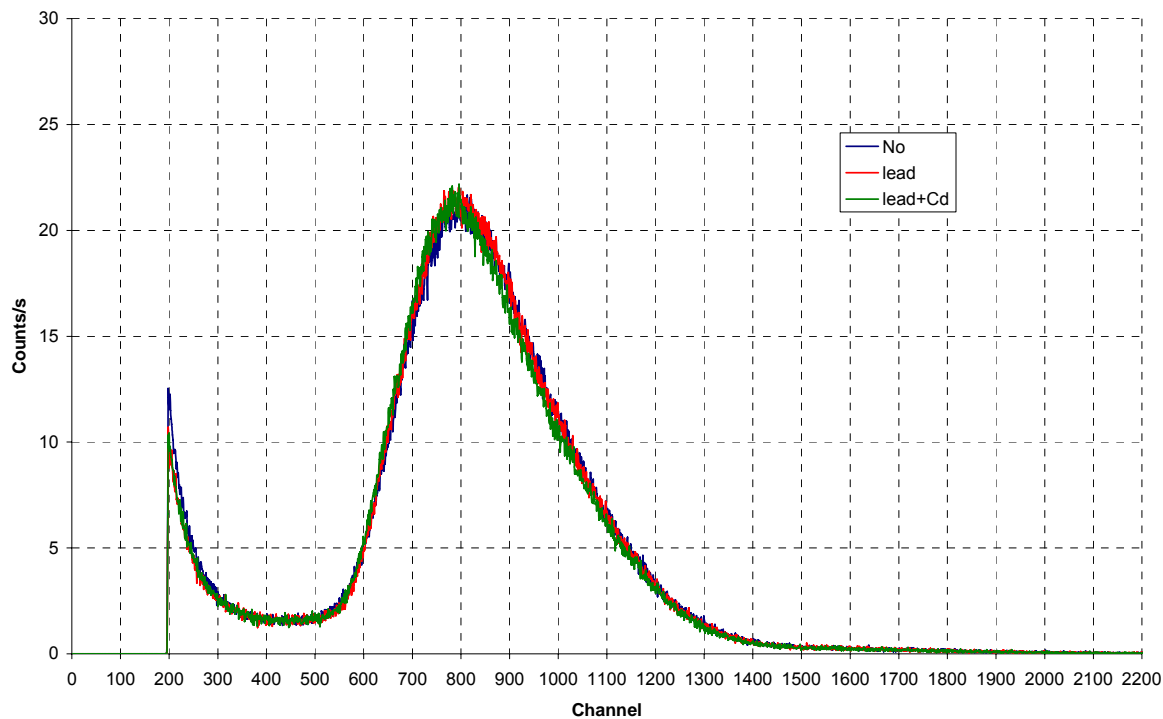


Figure 6: Pulse height spectra with and without lead and cadmium sheet

3.2 Measurements with Lead and Cadmium Sheets

Measurements using the 80 mils CH_2 thick polyethylene coated gallium arsenide detector facing the neutron beam were performed with and without lead and cadmium sheets. The lead sheet was 0.0125 inches thick and placed over the generator head to shield the gamma rays generated by the neutron source. The cadmium sheet was 20 mils thick and placed around the detector to shield the detector from thermal neutrons. The pulse height spectra for the 80 mils CH_2 thick detector with no shielding, with the lead sheet, and with the lead and cadmium sheets are shown in Figure 6.

As observed in Figure 6, the three measurements are virtually identical. With a lower level discriminator (LLD) set at channel 400, the integrated count rates differ by less than 0.5%. This demonstrates that the neutron-to-gamma ratio is greater than 200 to 1 and that the x-rays from the generator and $(n,2n)$ reactions in the lead sheet are negligible.

The ratio of integrated count rate above the lower energy threshold with and without cadmium is approximately 1.02. The detector response due to thermal neutrons is completely negligible and the cadmium ratio is actually a result of the resonances of cadmium at higher energies.

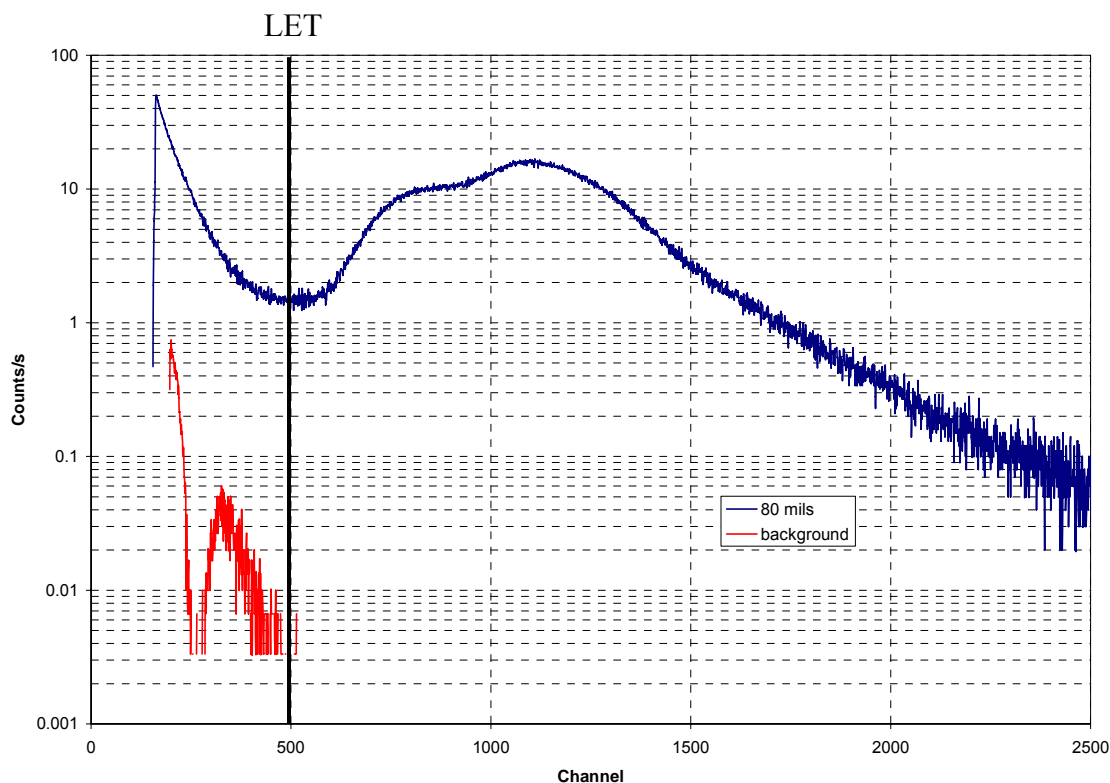


Figure 7: Background measurement

3.3 Background measurement

A background measurement was performed for each detector measurement. The background measured for the 80 mils CH₂ detector is compared with the signal of the detector in Figure 7. Above channel 200, the background is negligible and a lower energy threshold (LET) at channel 500 completely eliminates the background. For the other measurements, a lower energy threshold can always be selected where the background is negligible.

3.4 Effect of the high voltage

The relationship between the high voltage and the voltage measured on the gold contact depend on the detectors. The high voltage and the voltage at the gold contact was measured for the 1cm² square 2, 10 and 80 mils thick CH₂ detector and are listed in Table 4.

For the intrinsic efficiency and angular response measurements, the bias voltage is either 60 or 90 V, which means that the voltage at the contact varies between 10 and 30 V. The active length of GaAs is then on the order of 10 to 30 μm based on depletion depth values from literature of approximately 1 μm per V (ref. 2).

High voltage reading at power supply	Measured voltage across the detector contacts		
	2 mils CH ₂ detector	10 mils CH ₂ detector	80 mils CH ₂ detector
50	12.7	10.7	14.2
60	-	13.7	17.9
90	-	22.8	29.6
100	30.4	26.3	33.8
150	52.0	42.4	53.9
200	71.5	-	75.6

The evolution of the pulse height spectra with the bias voltage is studied by the “Bias voltage” series of measurements and shown in Figures 8 and 9 for the 1 cm² square, 10 and 80 mils CH₂ thick detectors.

When increasing the bias voltage, the pulse height spectrum is shifted towards the high energies and splits in two peaks. Increasing the bias voltage increases the thickness of the active region of GaAs where the charges are collected. The main charge carriers are the electrons which are collected on the Schottky contact (front gold contact). The holes are not collected by the ohmic contact (back gold layer) for the investigated bias voltages as they recombine within the inactive region of GaAs (ref. 2).

The peaks of the pulse height spectra can be fitted by Gaussian to determine their amplitudes and centroids. An example of the fit is shown in Figure 10 for the 1cm² square and 80 mils CH₂ thick detector operated at 100V.

The centroids of the two peaks increase linearly as a function of the bias voltage, but at different rates. For the investigated bias voltages, the active region increases linearly with the bias voltage (ref. 2). The two peaks correspond to the protons that deposit all their energy in the active region and the protons that have a range larger than the active region thickness and only deposit a portion of their energy. Increasing the bias voltage increases the thickness of the active region. By increasing the active region thickness, the former one will not deposit more energy but the charge collection will be enhanced whereas the latter one increases the amount of energy deposition as well, thereby leading to a faster increase. By increasing the active region thickness, more protons will deposit all their energy and thus the amplitude of the high energy peak (due to proton depositing a portion of their energy) will decrease faster than the low energy peak (due to proton depositing all their energy). This is experimentally observed in Figures 8 and 9.

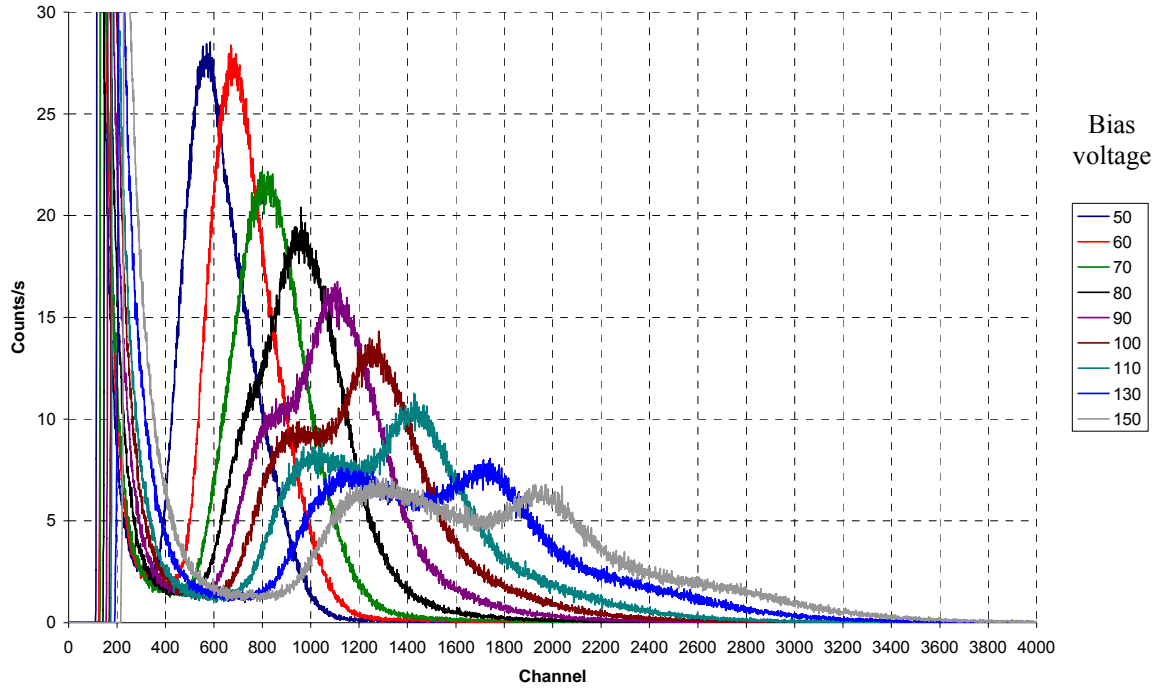


Figure 8: Pulse height spectra of the 1cm² square, 80 mils thick detector

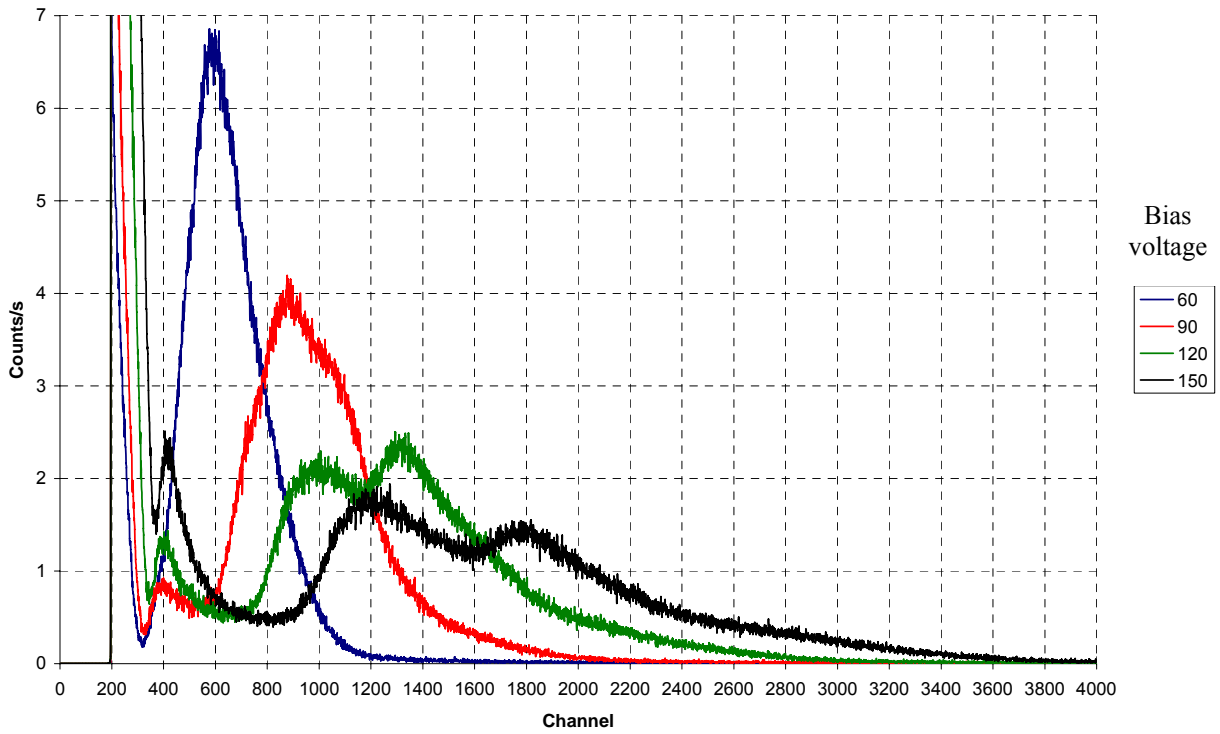


Figure 9: Pulse height spectra of the 1 cm² square, 10 mils thick detector

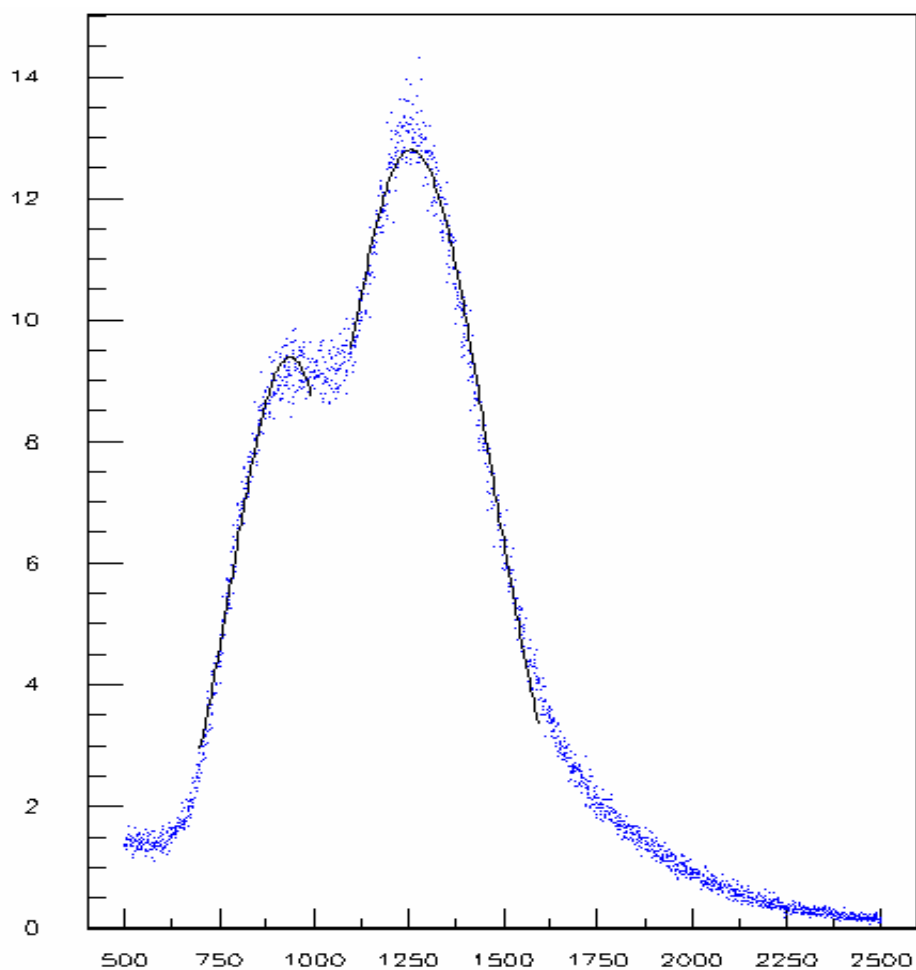


Figure 10: Example of gaussian fit of the pulse height spectra

Table 5: Integrated count rates for different high voltages		
Bias voltage (V)	Count rates (c/s)	
	10 mils CH ₂ detector	80 mils CH ₂ detector
50	-	9068 ± 10
60	2251 ± 3	8947 ± 10
70	-	8377 ± 10
80	-	8982 ± 10
90	2160 ± 3	9217 ± 10
100	-	9245 ± 10
110	-	8801 ± 10
120	2158 ± 3	-
130	-	8791 ± 10
150	2133 ± 3	8949 ± 10
Standard deviation	52	261

The integrated count rates above the lower energy threshold (necessary to discard electronic noise and low energy radiations) are listed in Table 5 for the 80 and 10 mils CH₂ thick detectors.

The integrated count rates have been normalized to the same number of source neutrons (using the ³He detector) for the 10 mils CH₂ detector and the standard deviation is lower than 3%. ³He monitoring was not performed for the 80 mils CH₂ detector which explains the high standard deviation. For the 10 and 80 mils detectors, the integrated count rates are however rather constant with the high voltage. Further investigation with detectors having a smaller thickness of CH₂ will be necessary to extend this conclusion.

3.5 Efficiency

The intrinsic efficiency of detectors normal to the neutron source has been investigated in the “Efficiency” series as a function of the thickness of the CH₂ layer. The 0.25 cm² round detector and the 1 cm² square detector were investigated.

The pulse height spectra for the 0.25 cm² round detector is shown in Figure 11 for different CH₂ thickness. The count rate increase from the 2 mils to the 80 mils CH₂ detector is clearly seen. The signal for the bare detector (without CH₂) is not completely negligible. This may be due to a thin plastic film used to protect the GaAs from impurities.

The absolute efficiency of the detector is obtained by normalizing the pulse height spectra to a constant neutron input by using the ³He tube, and by using the source strength determined previously. The intrinsic efficiency per unit area of the detector normal to the neutron source is deduced by dividing the absolute efficiency by the reduced solid angle $\Omega/4\pi$ and the surface of the detector. The uncertainties for the intrinsic efficiencies mainly refer to the uncertainty of the source strength measurement (approximately 9%). The intrinsic efficiencies per surface unit are listed in Table 6 and shown in Figure 12.

The intrinsic efficiency of the 0.25cm² and 1cm² detectors agrees within two standard deviations except for the 5 mils detector. An additional measurement with the 1cm² and 35 mils CH₂ layer detector will significantly improve the comparison.

CH ₂ thickness (mils)	1cm ² square - 41cm 90V ($\times 10^{-4}$ c/n/cm ²)	0.25cm ² round - 21cm 60V ($\times 10^{-4}$ c/n/cm ²)
bare	-	1.24 ± 0.12
2	4.72 ± 0.42	4.21 ± 0.38
5	8.79 ± 0.79	5.94 ± 0.53
10	11.3 ± 1.00	9.56 ± 0.85
35	-	21.4 ± 1.90
80	43.5 ± 3.9	31.7 ± 2.82

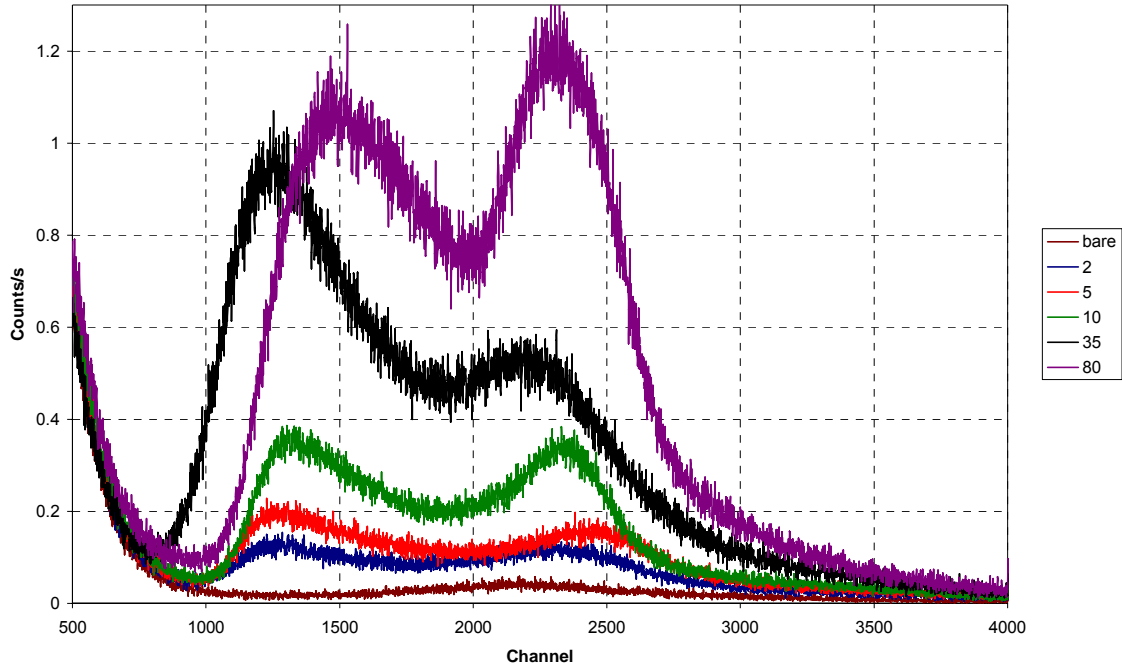


Figure 11: Pulse height spectra as a function of the CH₂ thickness

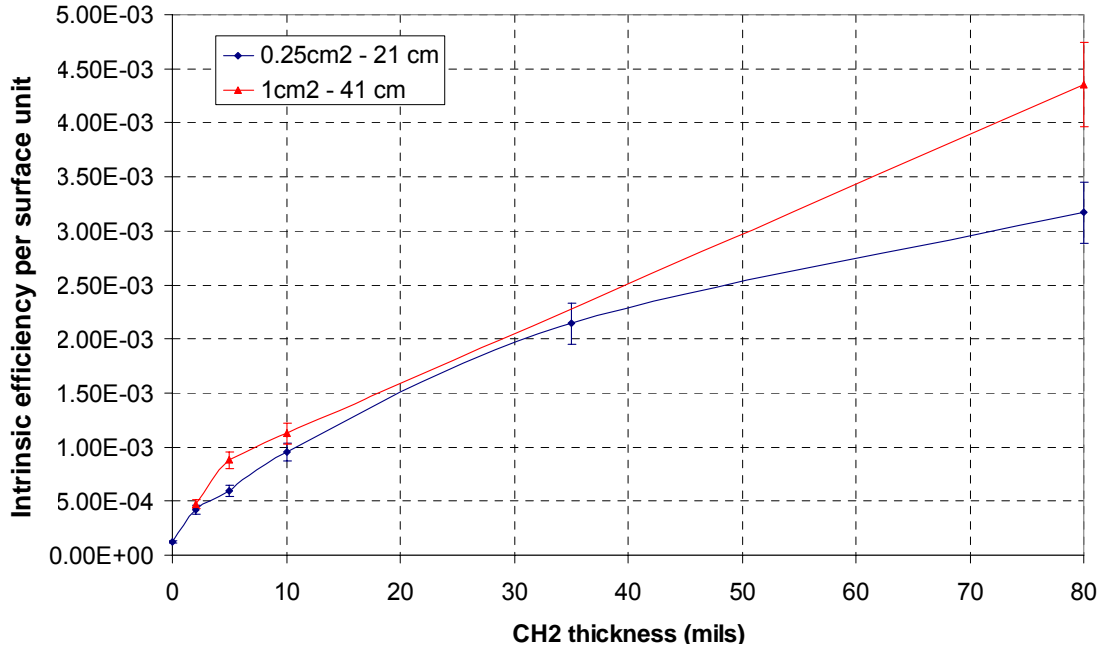


Figure 12: Measured absolute efficiency for different CH₂ thickness

3.6 Angular Response

The angular response of detectors has been investigated in the “Angular” series of tests. Angular response was measured for 1 cm² square detectors. Detectors with 2, 10 and 80 mils of CH₂ have been investigated at different distances from the neutron generator.

The pulse height spectra obtained for the 80 mils detector as a function of the angle with the neutron beam source is shown in Figure 13. The peak centroid shifts slightly towards the high energies and the deposited energy distribution broadens when increasing the angle of the detector with the normal to the neutron source.

The absolute efficiency is deduced from the pulse height spectra (normalized to the same neutron level) and the source strength determined in section 3.1. The angular response is expressed in terms of intrinsic efficiency per surface unit for a given angle of the detector normal to the neutron source. Practically, the absolute efficiency is divided by the reduced solid angle of the detector at 0 degree and the surface of the detector (see section 3.5). The angular response are listed in Table 7 and shown in Figure 14.

The uncertainties on the angular response refer mainly to the source strength uncertainty (approximately 9.0%). The uncertainty on the count rate integration is negligible (0.1%). The lower energy threshold selected to integrate the count rates depends on the detector. The uncertainty on the lower energy threshold is not considered.

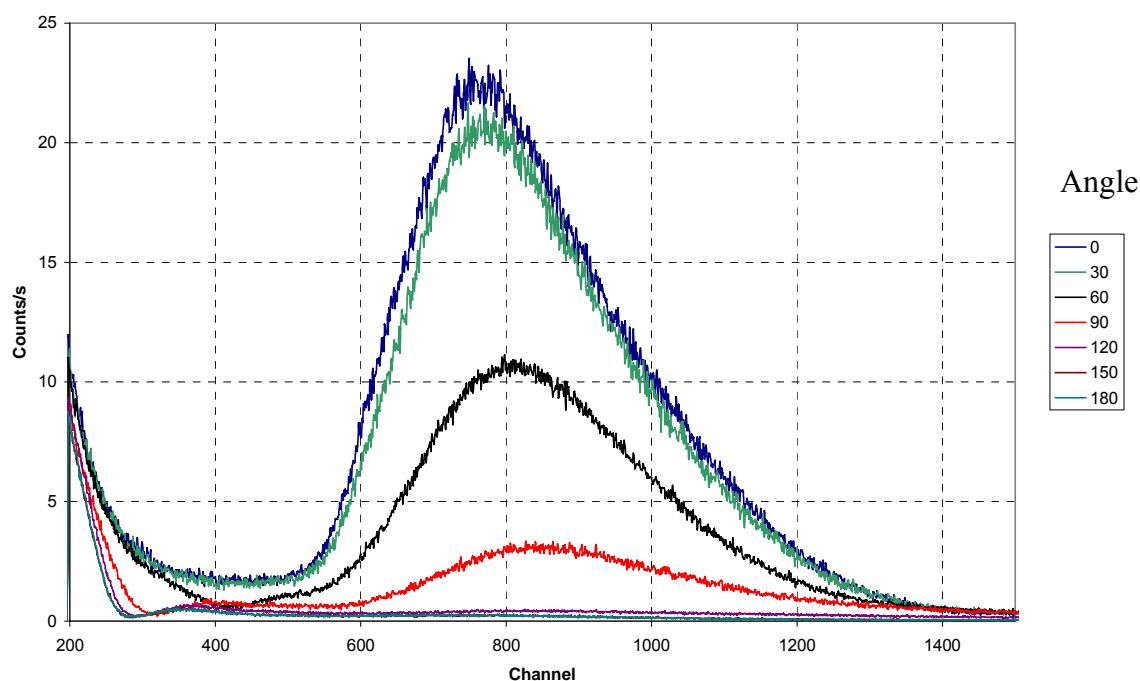


Figure 13: Pulse height spectra as a function of the detector angle with the neutron source beam

Table 7: Measured angular response					
Angle (degree)	2 mils CH ₂ 21cm 90V ($\times 10^{-5}$ c/n/cm ²)	10 milsCH ₂ 41cm 90V ($\times 10^{-5}$ c/n/cm ²)	80 mils CH ₂ 21cm 60V ($\times 10^{-5}$ c/n/cm ²)	80 mils CH ₂ 21cm 90V ($\times 10^{-5}$ c/n/cm ²)	80 mils CH ₂ 41cm 90V ($\times 10^{-5}$ c/n/cm ²)
0	3.87 ± 0.35	8.96 ± 0.80	31.6 ± 2.8	30.9 ± 2.8	34.7 ± 3.1
30	3.57 ± 0.32	8.39 ± 0.75	29.3 ± 2.6	28.7 ± 2.6	30.0 ± 2.7
45	3.25 ± 0.29	7.47 ± 0.67	-	22.4 ± 2.0	22.5 ± 2.0
60	-	6.00 ± 0.54	16.6 ± 1.5	-	15.6 ± 1.4
90	1.56 ± 0.14	3.33 ± 0.30	6.03 ± 0.54	5.48 ± 0.49	4.75 ± 0.43
120	0.95 ± 0.09	1.35 ± 0.12	1.47 ± 0.13	1.36 ± 0.13	1.49 ± 0.014
150	0.72 ± 0.07	-	0.61 ± 0.06	0.62 ± 0.06	0.75 ± 0.07
180	0.72 ± 0.07	0.71 ± 0.07	0.61 ± 0.06	0.60 ± 0.06	0.77 ± 0.07

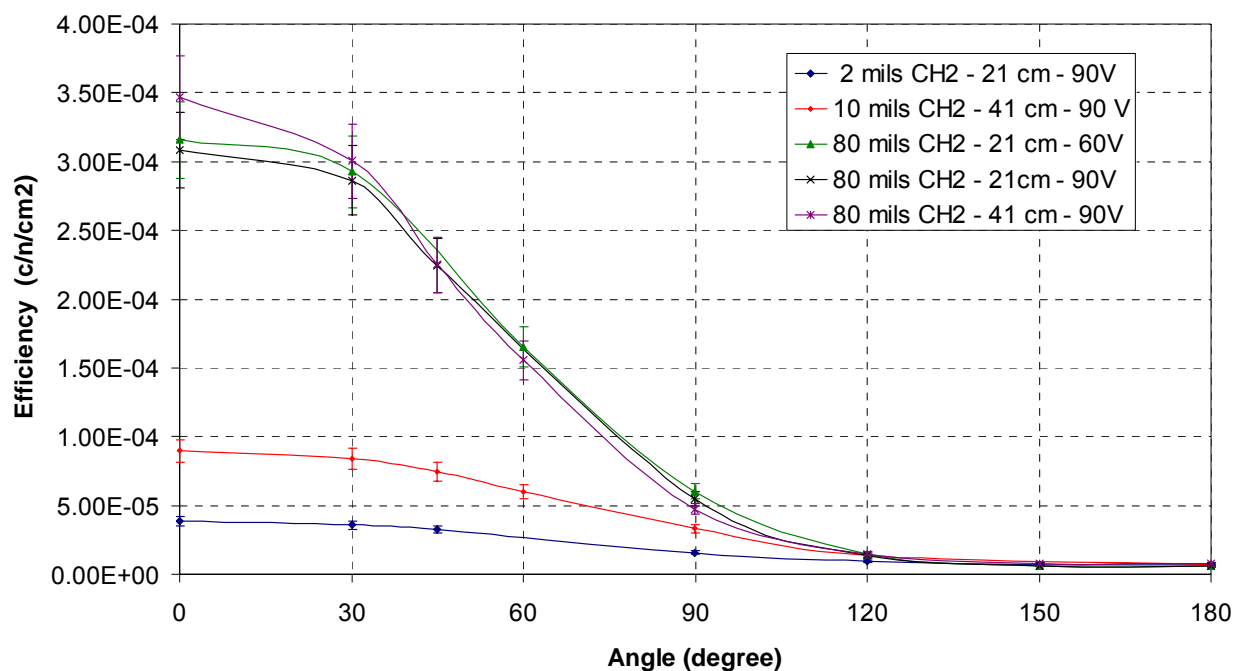


Figure 14: Measured angular response

The angular responses of the 80 mils detector are all in agreement at one standard deviation. The angular response of the 80 mils CH₂ detector measured at 21 cm from the neutron generator with a 60 and 90 V bias voltages are identical. The two series of measurements were performed on the same day by adjusting the bias voltage. The bias voltage had no influence on the integrated count rate results. For the rest of the report we will only consider the 90 V case.

The signal of the detectors at 180 degrees mainly depends on the distance between the detector and the neutron generator. The intrinsic efficiency should therefore be constant at 180 degree for all measurements performed at 21 and 41 cm. The intrinsic efficiency for the detector at the 180 degree angle differs by 15% for the measurement performed at 21 and 41 cm away from the neutron generator. For the 2 mils CH₂ thick detector, the intrinsic efficiency at 180 degree represents approximately 20% of the signal at 0 degree and is a major issue to interpret the measurements. For the 80 mils CH₂ thick detector, the signal of the detector at 180 degrees is only 2% of the signal at 0 degrees.

At 180 degrees, the signal cannot be generated by proton interaction in the GaAs layer because the active region does not stretch from the Schottky to the ohmic contact. Neutrons interacting with the gallium and arsenide nucleus can deposit energy through elastic, inelastic and radiative capture interactions. Because the mean free path of 14 MeV neutrons is much larger than the CH₂ layer, gold layers and GaAs layer, the main source of neutrons interacting with GaAs are 14 MeV neutrons and the number of interaction only depends on the neutron flux reaching the active region of GaAs. By moving the detector from 21 cm to 41 cm away from the neutron source, the incident flux of neutrons is approximately divided by 4. This is a good estimation of the factor 3 observed experimentally on the integrated counting rates. Accordingly, the number of neutron interactions should stay approximately constant for a detector positioned at different angles because the neutron flux on the detector volume remains the same. The neutron contribution to the detector signal can then be eliminated by subtracting the 180 degree measurement from measurements at other detector angles. The resulting efficiencies normalized to the 0 degree angle are shown in Figure 15.

The normalized efficiency does not account for the source strength and the uncertainty due to count rate statistics is negligible. There is however an uncertainty on the angle between the detector and the neutron beam which has not been evaluated but which is the major source of uncertainty.

The 2 and 10 mils CH₂ detectors normalized efficiency profiles are consistent because the proton sources induced by 14 MeV neutron reactions in a 2 or 10 mils thick CH₂ layer are comparable. Unexpectedly, the measurements at 21 and 41 cm using the 80 mils CH₂ detector are slightly different. A plus or minus 5 degree uncertainty on the angle normal to the neutron generator is shown in Figure 6 for the 80 mils detectors at 21 and 41 cm. The 5 degree uncertainty satisfactorily explains the difference between the two normalized responses.

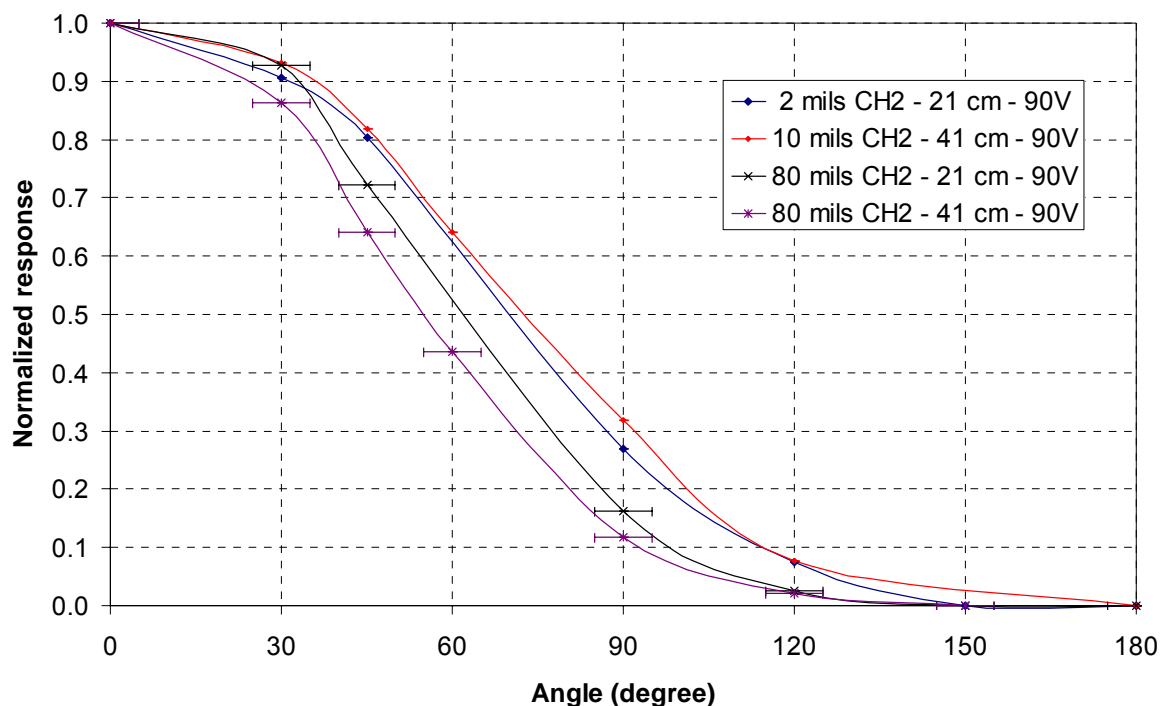


Figure 15: Normalized angular response with background subtraction

4 Calculations

The collected charge in the GaAs layer is mainly created by proton slowing down. The protons are created in the CH₂ layer by neutron scattering on the hydrogen nucleus. Possibly, alpha and ionized carbon nuclei can be created by 14 MeV neutron reactions on the carbon nuclei in the CH₂ layer. The ENDFB6.8 microscopic cross sections of interest for natural carbon and hydrogen are shown in Figure 16 and Figure 17.

The sum of elastic and inelastic scattering on the carbon nuclei is comparable to the elastic scattering on the hydrogen nucleus for 1 to 14 MeV neutrons. In CH₂, protons issued from elastic scattering on hydrogen are at least two times more probable than ionized carbon nuclei created by elastic and inelastic scattering. The mean free path of carbon nucleus is also approximately 36 times smaller than that of the proton (ref. 3) forbidding carbon nuclei to reach the active region. Therefore, the ionized carbon nuclei do not significantly contribute to the detector response.

Similar arguments hold for the alpha generated by (n,α) reactions on the carbon nucleus. The microscopic cross section is 10 times lower and the mean free path of alpha particle is 4 times lower than for the proton.

Neutrons that have not interacted with the CH₂ layer and the gold contact can deposit energy in the GaAs. This contribution is not completely negligible especially for detectors with a small CH₂ layer at 150 or 180 degrees (see section 3.6).



Figure 16: ENDFB6.8 cross sections for natural carbon

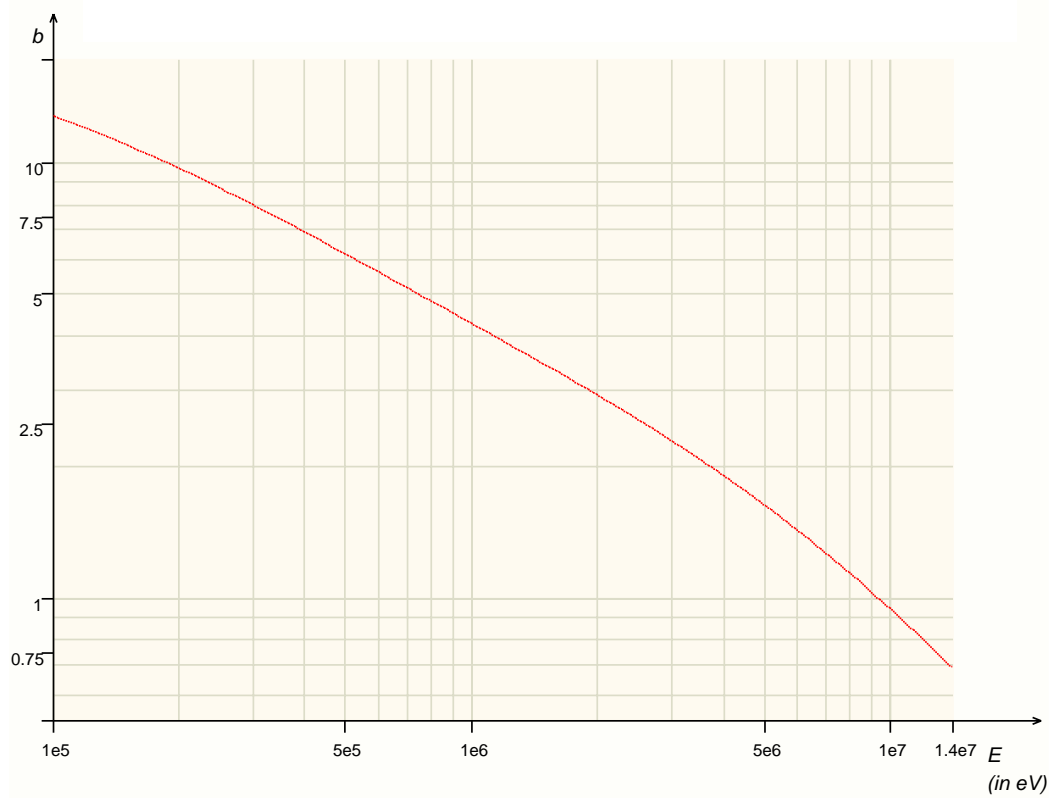


Figure 17: ENDFB6.8 elastic scattering cross section for hydrogen

The MCNPX-2.5 code system was used to calculate the energy deposition in the GaAs. Neutrons and protons, issued from elastic collision of neutrons on the hydrogen nucleus, are transported. A pulse height tally (F8) is used to determine the energy deposition in the active region of GaAs. Because of the non analog transport of neutrons, pulse height tallies for neutron energy deposition should be avoided and only the total energy deposition due to protons is accurate (ref. 4). Therefore, the pulse height tally is used to determine the energy deposited by protons having energy greater than 100keV.

The GaAs active length, where the energy deposition occurs, depends on the bias voltage on the detector. If the bias voltage is greater than 20V, the active length of GaAs increases linearly with the bias voltage with approximately $1\mu\text{m}/\text{V}$ (ref. 2). The detector bias voltages range from 20 to 30V and the active length is therefore 20 to 30 μm (see section 2.2.3). For a 20 μm thick active region, all protons deposited more energy than the lower energy threshold (100 keV), therefore increasing the active length does not change the number of detected protons.

The neutron contribution is not calculated but deduced from the experiment when possible. The signal of detectors being rotated at 180 degrees is mainly due to neutron interaction in the GaAs. Because the neutron signal should not vary significantly with the detector angle, we use the signal at 180 degrees as a measure of the detectors response based on this effect. The calculated values that only account for the energy deposition due to protons can then be corrected by the measured energy deposition by neutrons (see section 3.6).

5 Comparisons

5.1 Efficiency

The comparison between calculated and measured intrinsic efficiency is difficult to perform because of the lack of information on the source strength during the measurement (see section 3.1) and the inaccuracy of neutron pulse height tally in MCNP (see section 4).

The measured and calculated intrinsic efficiencies are listed in Table 8 and shown in Figure 18 for the 0.25 cm^2 round and 1 cm^2 square detectors at 0 degree angle. Uncertainties on the measurements are mainly due to the uncertainty on the source strength ($\sim 9\%$).

CH ₂ thickness (mils)	1cm ² square - 41cm - 90V ($\times 10^{-4}$ c/n/cm ²)			0.25cm ² round - 21cm - 60V ($\times 10^{-4}$ c/n/cm ²)		
	Measured	Calculated	C/E	Measured	Calculated	C/E
2	4.72 \pm 0.42	2.99 \pm 0.03	0.634 \pm 0.057	4.21 \pm 0.38	3.84 \pm 0.03	0.912 \pm 0.081
5	8.79 \pm 0.79	5.96 \pm 0.04	0.678 \pm 0.060	5.94 \pm 0.53	6.91 \pm 0.04	1.163 \pm 0.103
10	11.3 \pm 1.00	10.3 \pm 0.05	0.915 \pm 0.081	9.56 \pm 0.85	11.4 \pm 0.05	1.189 \pm 0.109
35	-	25.5 \pm 0.07	-	21.4 \pm 1.90	26.3 \pm 0.08	1.227 \pm 0.109
80	43.5 \pm 3.9	35.9 \pm 0.08	0.825 \pm 0.073	31.7 \pm 2.82	36.1 \pm 0.09	1.140 \pm 0.101

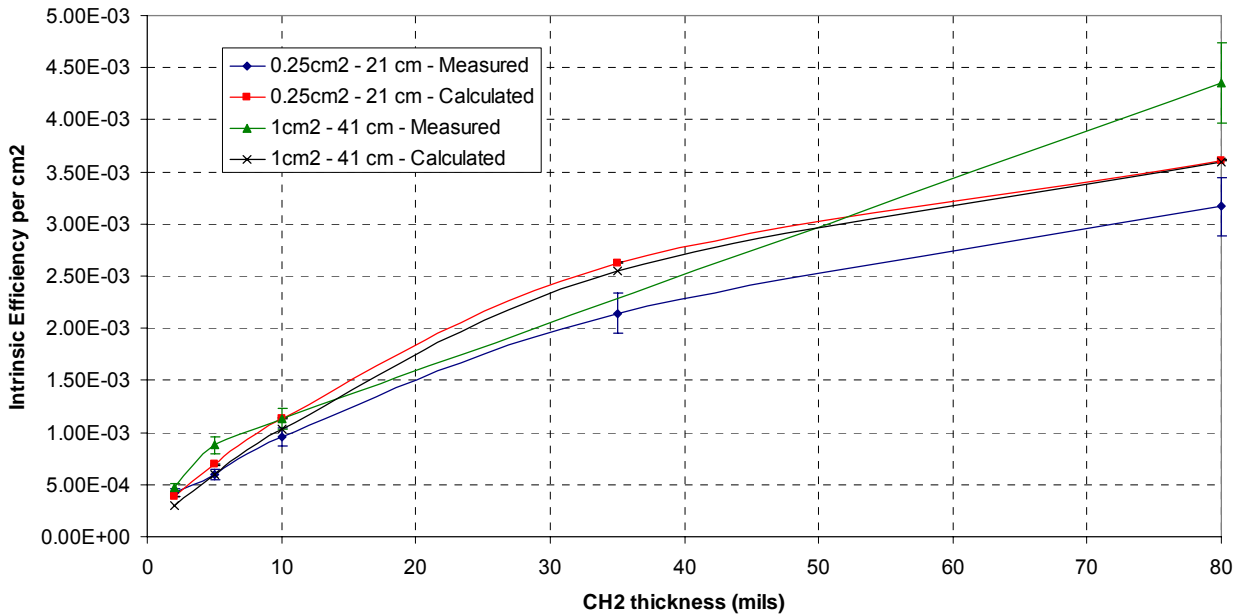


Figure 18: Intrinsic efficiency of the 0.25 cm² round and 1 cm² square detectors

The calculated intrinsic efficiency of the 0.25 cm² and 1 cm² detectors are similar. There are more differences between the two experimental profiles. Because the source strength is unknown, the measured curves can be scaled by a constant factor and, depending on that factor, the calculation values may satisfactorily predict one of the two experimental curves.

5.2 Angular response

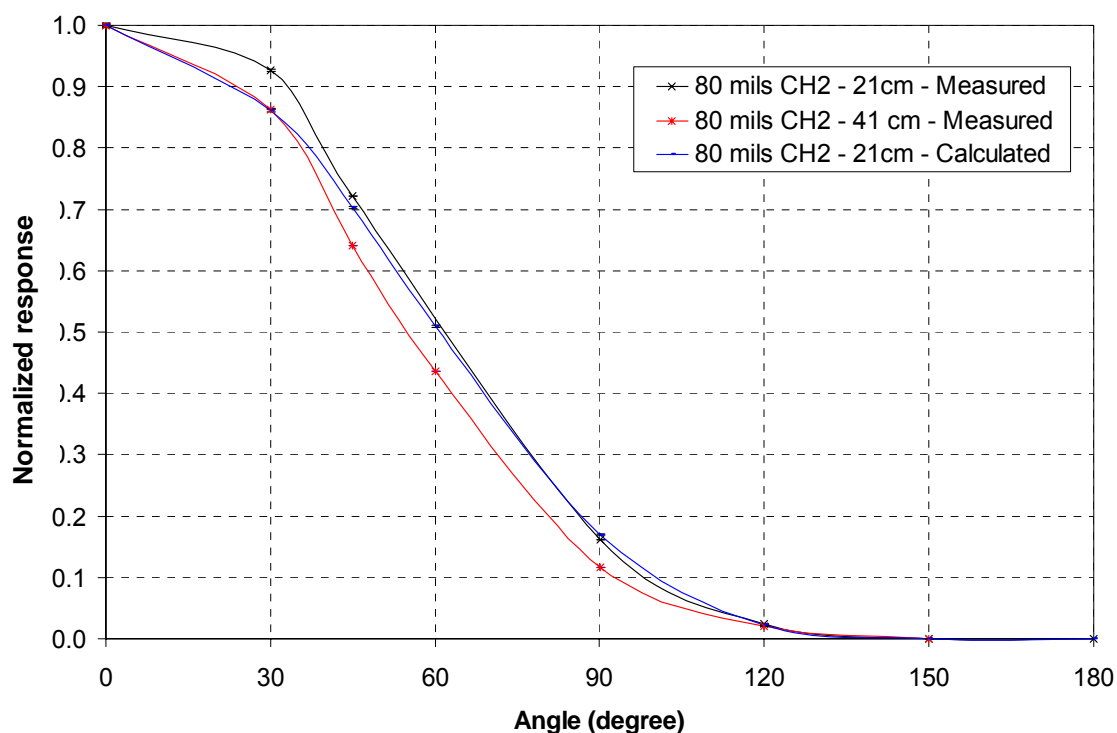
The comparison between measurements and calculations is performed in two steps. First, the calculated and measured normalized efficiencies due to proton interactions in GaAs are compared. Second, the measured and calculated intrinsic efficiencies per unit area are compared.

Comparing the normalized efficiencies due to protons, allows one to eliminate the issues of neutron interactions in the GaAs, which are not taken into account in the calculations (see section 4), and of source strength, which is not precisely known during the measurements (see section 3.1).

The measured normalized efficiency for protons are obtained by subtracting the signal of the detector at 180 degrees from the other signal to eliminate the neutron signal and then normalized to the value at 0 degree. The calculations are only normalized to the value at 0 degree. The resulting normalized efficiencies are listed in Table 9 and shown in Figure 19 for the 80 mils detectors at 21 and 41 cm from the source, and in Table 10 and Figures 8 and 9 for the 2 and 10 mils detectors.

Angle (degree)	80 mils CH ₂ - 21cm		80 mils CH ₂ - 41cm	
	Measured	Calculated	Measured	Calculated
0	1.000	1.000	1.000	1.000
30	0.927 ± 0.001	0.861 ± 0.003	0.864 ± 0.001	0.859 ± 0.003
45	0.722 ± 0.001	0.703 ± 0.003	0.641 ± 0.001	0.699 ± 0.003
60	-	0.509 ± 0.003	0.436 ± 0.001	0.506 ± 0.002
90	0.161 ± 0.001	0.169 ± 0.002	0.117 ± 0.001	0.165 ± 0.001
120	0.025 ± 0.001	0.022 ± 0.001	0.021 ± 0.001	0.021 ± 0.001
150	0.000 ± 0.001	0.000 ± 0.001	-	0.000 ± 0.001

Angle (degree)	2 mils CH ₂ - 21cm		10 mils CH ₂ - 41cm	
	Measured	Calculated	Measured	Calculated
0	1.000	1.000	1.000	1.000
30	0.906 ± 0.002	0.953 ± 0.013	0.931 ± 0.002	0.944 ± 0.006
45	0.804 ± 0.002	0.879 ± 0.012	0.819 ± 0.002	0.866 ± 0.005
60	-	0.768 ± 0.011	0.642 ± 0.002	0.744 ± 0.005
90	0.269 ± 0.001	0.459 ± 0.007	0.318 ± 0.001	0.400 ± 0.003
120	0.074 ± 0.001	0.176 ± 0.004	0.078 ± 0.001	0.073 ± 0.001
150	0.001 ± 0.001	0.003 ± 0.001	-	0.001 ± 0.001

Figure 19: Measured and calculated normalized efficiency of the 80 mils thick CH₂ layer detector

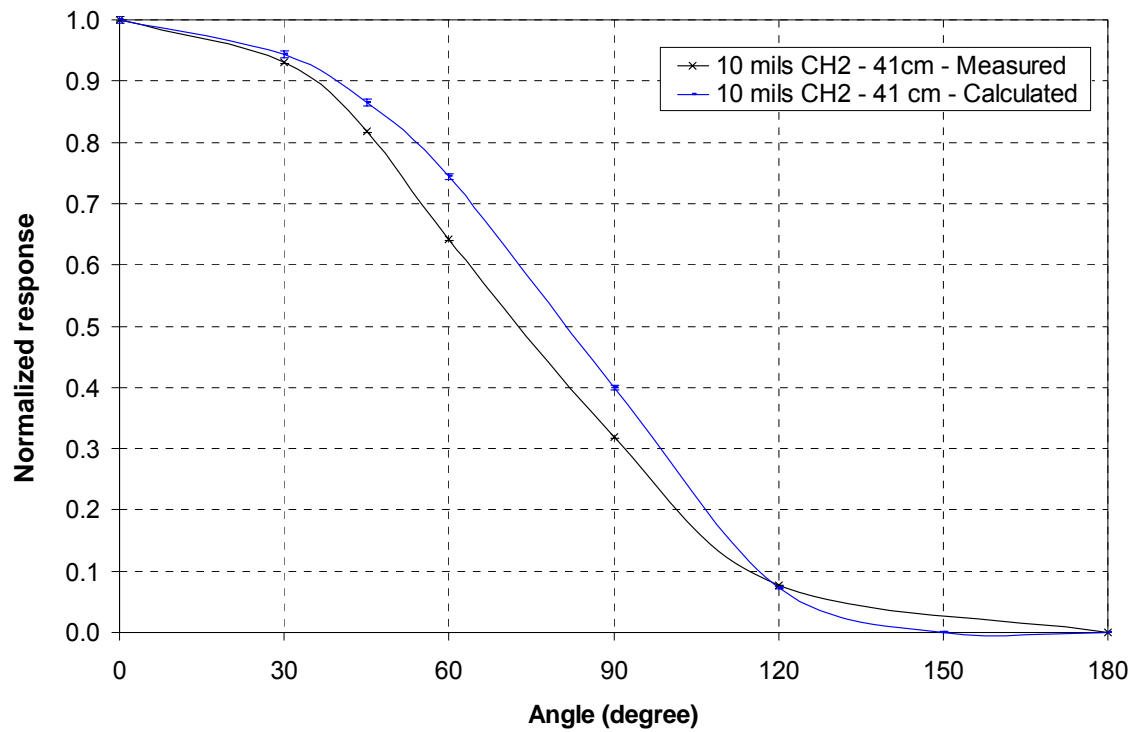


Figure 20: Measured and calculated normalized efficiency of the 10 mils CH₂ layer detector

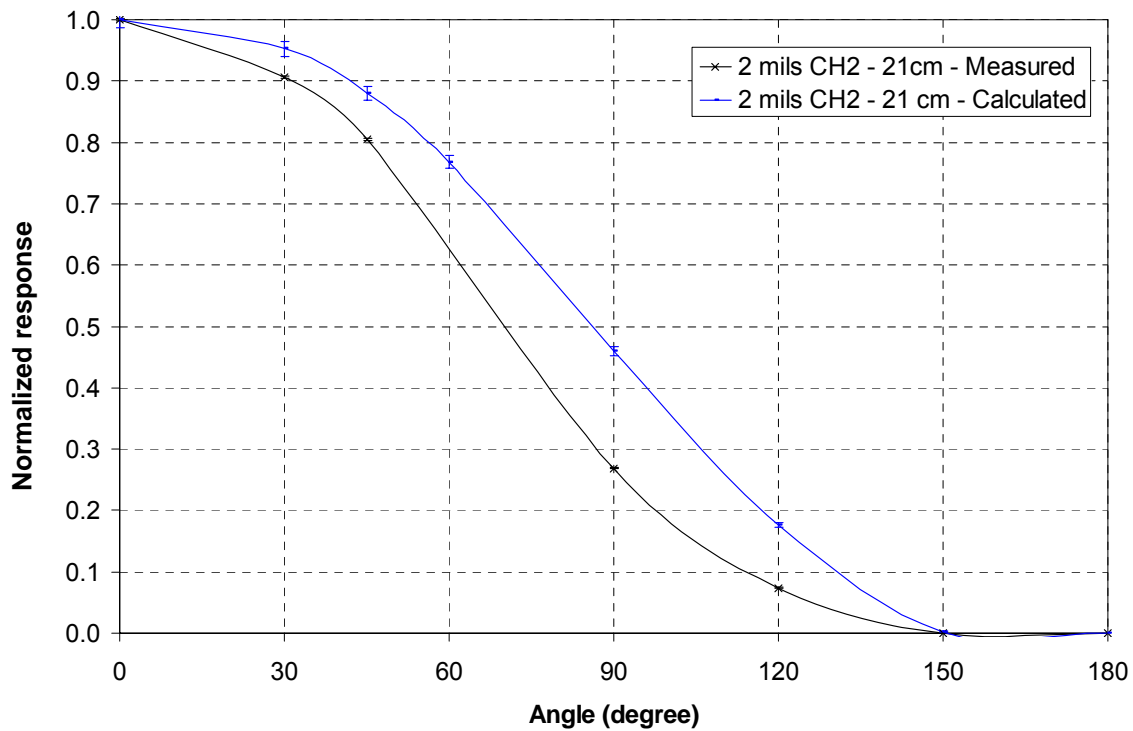


Figure 21: Measured and calculated normalized efficiency of the 2 mils thick CH₂ layer detector

The statistical uncertainties on the calculated and measured values are almost negligible in every case. The uncertainty on the angle of the detector normal to the neutron beam and on the detector distance is not taken into account for the measured values, but should be considered.

The 80 mils CH₂ thick layer detector responses calculated at 21 and 41 cm are identical within the uncertainty (Table) and the calculated value at 21 cm is the only one plotted in Figure 10. The agreement between the measured and calculated values for the 80 mils CH₂ detector is excellent except for the 30 degree angle.

The calculations also tend to overestimate the measured values for the 10 and 2 mils detectors. The smaller the polyethylene layer, the greater the overestimation.

The measured absolute efficiency is deduced from the measured counting rates and the source strength value during each measurement. To be able to compare the measured and calculated absolute efficiencies we have to choose a source strength level common to all measurements. The error on that level is unknown (see section 3.1). Moreover, the calculations have been corrected for the neutron energy deposition in the GaAs by using the measurement value at 180 degrees.

The calculated and measured angular absolute efficiencies are listed in Tables 11 and 12, and shown in Figures 22 and 23.

Angle (degree)	80 mils CH ₂ - 21cm ($\times 10^{-5}$ c/n/cm ²)			80 milsCH ₂ - 41cm ($\times 10^{-5}$ c/n/cm ²)		
	Measured	Calculated	C/E	Measured	Calculated	C/E
0	30.9 ± 2.8	28.9 ± 0.09	0.938 ± 0.083	34.7 ± 3.1	29.4 ± 0.10	0.847 ± 0.075
30	28.7 ± 2.6	25.0 ± 0.09	0.873 ± 0.078	30.0 ± 2.7	25.3 ± 0.10	0.843 ± 0.075
45	22.4 ± 2.0	20.5 ± 0.08	0.914 ± 0.081	22.5 ± 2.0	20.7 ± 0.09	0.922 ± 0.082
60	-	15.0 ± 0.08	-	15.6 ± 1.4	15.2 ± 0.09	0.980 ± 0.087
90	5.48 ± 0.49	5.40 ± 0.06	0.985 ± 0.088	4.75 ± 0.43	5.48 ± 0.08	1.153 ± 0.104
120	1.36 ± 0.13	1.21 ± 0.06	0.890 ± 0.089	1.49 ± 0.014	1.37 ± 0.07	0.918 ± 0.094
150	0.62 ± 0.06	0.61 ± 0.06	0.993 ± 0.124	0.75 ± 0.07	0.79 ± 0.07	1.043 ± 0.130
180	0.60 ± 0.06	0.60 ± 0.06	1.000 ± 0.126	0.77 ± 0.07	0.77 ± 0.07	1.000 ± 0.126

Angle (degree)	2 mils CH ₂ - 21cm ($\times 10^{-5}$ c/n/cm ²)			10 milsCH ₂ - 41cm ($\times 10^{-5}$ c/n/cm ²)		
	Measured	Calculated	C/E	Measured	Calculated	C/E
0	3.87 ± 0.35	2.60 ± 0.07	0.672 ± 0.062	8.96 ± 0.80	8.65 ± 0.08	0.965 ± 0.086
30	3.57 ± 0.32	2.51 ± 0.07	0.703 ± 0.065	8.39 ± 0.75	8.21 ± 0.08	0.978 ± 0.087
45	3.25 ± 0.29	2.37 ± 0.07	0.730 ± 0.068	7.47 ± 0.67	7.58 ± 0.08	1.016 ± 0.091
60	-	2.16 ± 0.07	-	6.00 ± 0.54	6.62 ± 0.07	1.102 ± 0.099
90	1.56 ± 0.14	1.58 ± 0.07	1.011 ± 0.099	3.33 ± 0.30	3.88 ± 0.07	1.165 ± 0.105
120	0.95 ± 0.09	1.05 ± 0.07	1.104 ± 0.089	1.35 ± 0.12	1.28 ± 0.07	0.953 ± 0.097
150	0.72 ± 0.07	0.73 ± 0.07	1.003 ± 0.126	-	0.71 ± 0.07	-
180	0.72 ± 0.07	0.72 ± 0.07	1.000 ± 0.126	0.71 ± 0.07	0.71 ± 0.07	1.000 ± 0.126

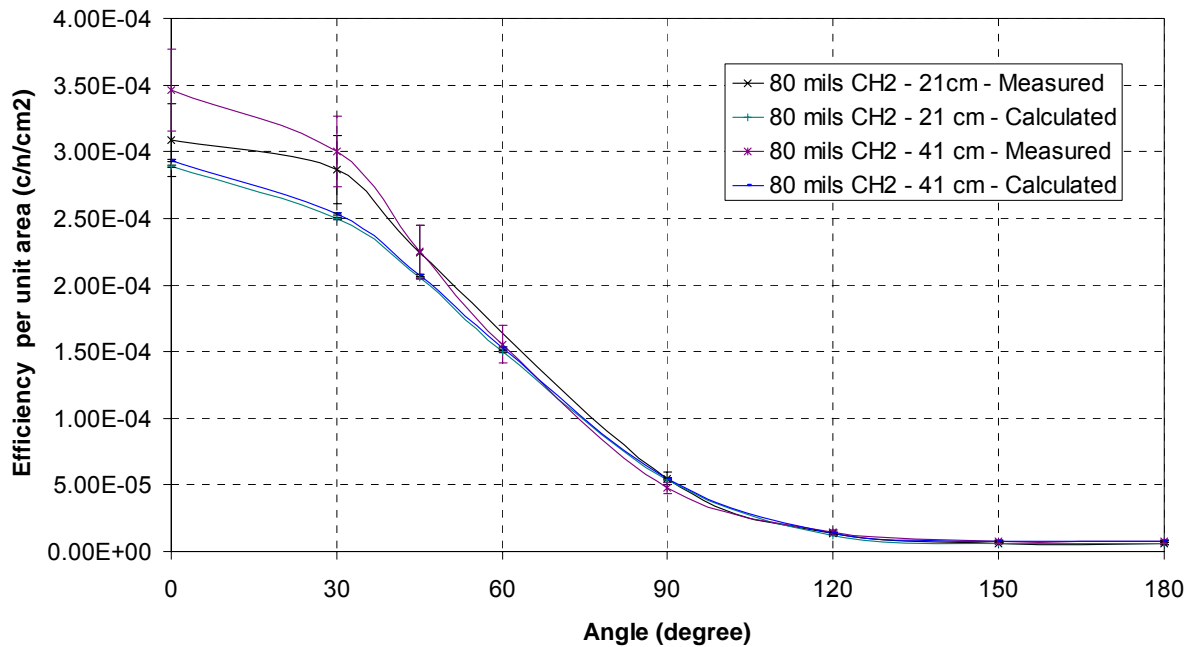


Figure 22: Measured and calculated absolute angular efficiency of the 80 mils CH2 detector

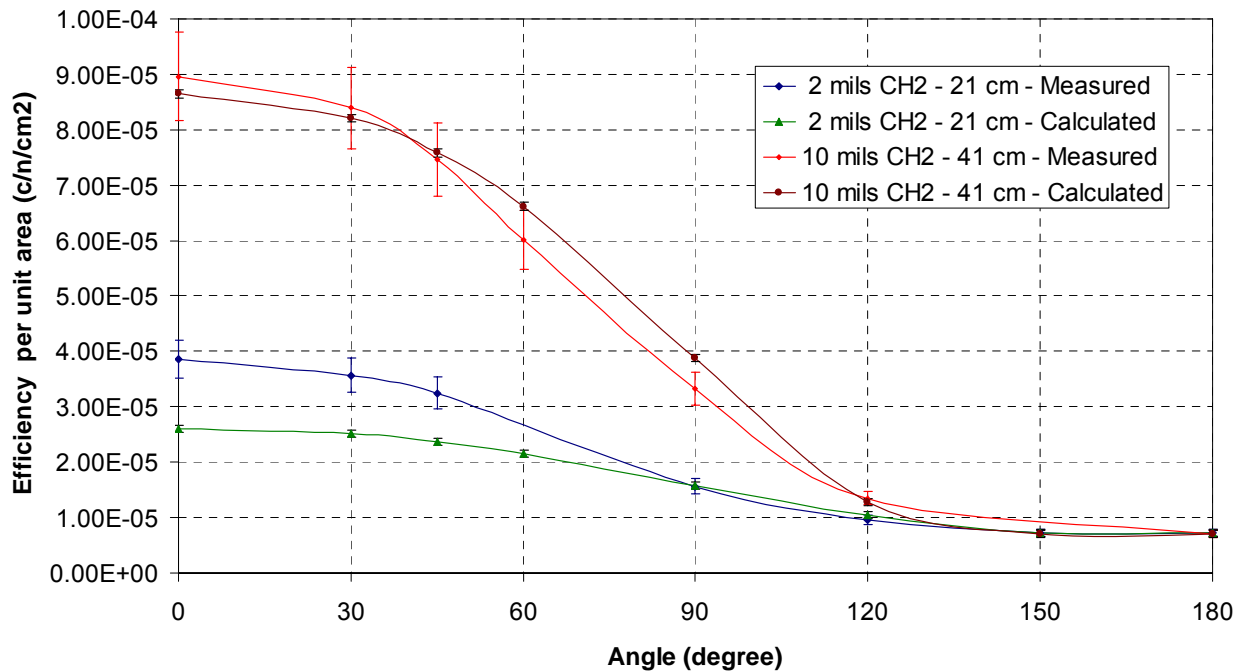


Figure 23: Measured and calculated absolute angular efficiency of the 2 and 10 mils CH2 detectors

The uncertainty of the measured values is mainly a result of the 9% uncertainty on the source strength measurement. The absolute efficiency of the 2 mils detector is not well predicted whereas the calculated estimations for the 10 and 80 mils agree with the experimental values at one or two standard deviations.

6 Conclusion

Once corrected for the energy deposition of neutrons in the GaAs, the calculated angular efficiencies overestimate the experimental profiles. The overestimation increases as the CH₂ thickness decreases. For 80 mils CH₂ thick layer detectors, the overestimation is lower than 7% and the measured and calculated values agree nicely. Because of their low efficiencies, the 2 and 10 mils detectors are not adapted to a 14 MeV neutron source. The 10 mils thick CH₂ detector used for further measurement with a fission neutron source (mean energy of 1MeV) should present similar characteristics as the 80 mils detector with a 14 MeV neutron source and the calculation will be able to correctly predict the relative angular efficiency.

The measured and calculated absolute efficiency are also in agreement at 2 standard deviations for the 80 and 10 mils CH₂ detectors. Nevertheless, knowing the neutron source strength is required to eliminate any potential scaling factor for the measured efficiencies. The conclusion applies to the efficiency determined at 0 degree for different CH₂ thick layer and to the angular efficiencies.

Polyethylene-coated gallium arsenide detectors were studied because the detection scheme is based on measuring the signal in the gallium arsenide wafers from the electrical charge of the recoil protons produced from the scattering of neutrons from the hydrogen nucleus. The inherent reaction has a directional dependence because the neutron and hydrogen nucleus have equivalent masses.

The assessment and measurement of polyethylene-coated gallium arsenide detector properties and characteristics was the first phase of a project being performed for the Department of Homeland Security. The ultimate goal of the project was to develop a man-portable neutron detection system that has the ability to determine the direction of the source from the detector.

The efficiency of GaAs detectors for different sizes of polyethylene layers and different angles between the detector and the neutron source were determined. Preliminary measurements with a neutron generator based on a deuterium-tritium reaction (~14 MeV neutrons) were performed and the results presented. Comparison of the measurement results to Monte Carlo calculations allowed the validation of the calculation scheme so that modeling can be used in the future to design an integrated detector system and predict detection results without having to perform significant additional measurements.

Based on the results of this study, the polyethylene-coated gallium arsenide detectors provide adequate angular resolution based on proton recoil detection from the neutron scattering reaction from hydrogen. However, the intrinsic efficiency for an individual detector is extremely low. Because of this low efficiency, large surface area detectors (or a large total surface area from

many small detectors) would be required to generate adequate statistics to perform directional detection in near-real time to make it practical for rapid search applications. Large surface areas could be created by stacking the detector wafers with only a negligible attenuation of source neutrons. However, the cost of creating such a large array of GaAs is considered cost-prohibitive at this time.

References

1. D. Reilly, N. Ensslin, and H. Smith, Jr., Passive Nondestructive Assay of Nuclear Materials, U.S. Nuclear Regulatory Commission Report NUREG/CR-5550, March, 1991.
2. C.M. Buttar, GaAs detectors – A review, Nuclear Instruments and Methods A 395 (1997) 1-8
3. G.F. Knoll, Radiation detection and measurement, New York, Wiley 1989
4. J.F. Briesmeister, MCNPTM – A General Monte Carlo N-Particle Transport Code (Version 4C), LA-13709-M.

Appendix 1:

**Argonne National Laboratory Intra-Laboratory Memorandum
on the Output of the MF-Physics A-711 Neutron Generator**

**ARGONNE
NATIONAL
LABORATORY**
INTRA-LABORATORY MEMO

November 14, 2002

TO: Michael Zacher NRAD Reactor Manager

FROM: Jeff Sanders Nuclear Engineer, Nuclear Technology Division

SUBJECT: **Reassessment of the average neutron energy and flux levels of the MF-Physics A-711 Neutron Generator**

The average neutron energy and flux levels produced by the MF-Physics A-711 Neutron Generator were reanalyzed using nickel (Ni) and aluminum (Al) foil irradiation data as well as data from a recently completed iron (Fe) foil irradiation. Besides the addition of the Fe foil activation data, the reanalysis differs from the previous (August 2002) analysis in that:

- The $^{27}\text{Al}(n,p)^{27}\text{Mg}$ reaction was not used in the reanalysis because of the precise timing necessary due to the short half-life (9.462 minutes) of the reaction
- The $^{56}\text{Ni}(n,p)^{58}\text{Co}$ reaction was used in the reanalysis of the neutron energy and flux near the head of the generator
- The earlier Ni foil irradiation data was corrected to account for inconsistencies between predicted and observed decay times
- Copper foil irradiation data was not used

The reanalysis was performed as prescribed by the ASTM E 496-96 Standard Test Method. The three foils were irradiated under the conditions shown in Table 1.

Table 1: Irradiation conditions for Al, Fe and Ni foils

<i>Foil Type</i>	<i>Generator Energy</i>	<i>Distance from Head</i>	<i>Irradiation Time</i>
Ni	150 kV, 2.5 mA	near head, on centerline	60 minutes
Ni	150 kV, 2.5 mA	12 in from head, on centerline	60 minutes
Al	150 kV, 2.5 mA	near head, on centerline	20 minutes
Al	150 kV, 2.5 mA	12 in from head, on centerline	20 minutes
Fe	150 kV, 2.5 mA	near head, on centerline	60 minutes
Fe	150 kV, 2.5 mA	12 in from head, on centerline	60 minutes

The saturation activity per target atom for the neutron activation products ^{57}Ni , ^{58}Co , ^{24}Na and ^{56}Mn were calculated. By taking a ratio of the saturation activities shown below, the cross section ratios were determined, allowing the determination of neutron energy by interpolation of ENDF VI cross section data.

$$\frac{^{58}\text{Ni}(n,p)^{58}\text{Co}}{^{58}\text{Ni}(n,2n)^{57}\text{Ni}} \quad \frac{^{27}\text{Al}(n,\alpha)^{24}\text{Na}}{^{58}\text{Ni}(n,2n)^{57}\text{Ni}} \quad \frac{^{56}\text{Fe}(n,p)^{56}\text{Mn}}{^{58}\text{Ni}(n,2n)^{57}\text{Ni}}$$

Using the average neutron energy determined from each of the reaction ratios, the neutron flux at twelve inches and on the face of the generator was calculated. The results are summarized below. Both the average neutron energy and flux are within two standard deviations of the measurement performed with only the Al and Ni foils (August 2002), though it is believed that the reanalyzed results are more representative of the actual levels because of the additional Fe foil data. Tables 3 through 6 summarize the details of the neutron and energy flux determination.

Table 2: Summary of neutron energy and flux levels calculated for the MF-Physics A-711 Neutron Generator (theoretical errors due to counting statistics in parenthesis, operated at 150 kV, 2.5 mA)

<i>Distance from Head</i>	<i>Neutron Energy (MeV)</i>	<i>Flux ($n \cdot cm^{-2} \cdot s^{-1}$)</i>
near head	$14.42 \pm 0.46\%$ (0.41%)	$7.97 \times 10^8 \pm 4.90\%$ (4.18%)
12 in from head	$14.64 \pm 3.48\%$ (0.92%)	$1.35 \times 10^6 \pm 18.82\%$ (1.25%)

The Ni foil irradiation at 12" was not performed long enough for a measurement of the ^{58}Co activity to be determined, so this reaction was neglected in the reanalysis of the neutron energy and flux at 12" from the head. It is important to note that the uncertainties in energy and flux presented in parenthesis in Table 2 are the theoretical errors due to counting statistics and cross section uncertainties alone, while those outside the parenthesis are the observed statistical errors. The large deviation in observed statistical error with respect to theoretical error at 12" from the head is most likely a result of errors in the background correction performed during the gamma spectroscopy analysis as well as timing inaccuracies. Due to the low count rates, small errors in background correction will result in large errors in the saturation activity calculation. These errors are not accounted for in the theoretical error calculation. The best approach to reducing both the overall error and difference in observed and theoretical error is to increase the irradiation time for irradiations performed at distances from the head. Increasing the irradiation time for foils placed at 10-50cm to 4-6 hours is recommended for improved accuracy. Incorporating the use of a stopwatch or other accurate timing instrument throughout the course of the measurements would decrease the effects of timing errors, perhaps allowing the use of the $^{27}\text{Al}(n,p)^{27}\text{Mg}$ reaction in the analysis. If accurate timing can be performed, this reaction has a high specific activity that will reduce the error associated with counting statistics in most circumstances.

The neutron flux levels produced by the neutron generator are related to the operating parameters as well as the age of the head. The neutron energy and flux levels were measured near the beginning of the head lifetime, and the flux was determined to be proportional to the inverse of the squared distance from a point 1cm within the generator head. This finding allowed the neutron source to be treated as an isotropic point source located within the head. The current measurements do not support this finding, most likely a result of the target material being sputtered throughout the lifetime of the head. This sputtering is the main cause of decreased neutron flux levels and appears to also enlarge the source region. From the reanalyzed flux measurements, this region is roughly estimated to be circular with a diameter of 0.5 cm. Since the size of this region will change during the lifetime of the generator head, it is suggested that the flux levels be measured both at the face of the head and at an irradiation position 10-50cm from the head every 100-200 mA-hours using the Al, Ni and Fe foils.

Due to the age of the current head, it is further suggested that a new head be obtained prior to any extensive irradiation campaign. The current head has been operated for nearly 250 hours at a current of 2.5 mA. While the expected lifetime of the tube is around 300 hours at this operating level (per manufacturer), alterations to the generator to allow it to operate in a pulsing mode decrease this expected lifetime. When operated in this mode, the lifetime of the tube decreases to around 100 operating hours.

Since the tube has been operated in both pulsing and steady beam mode, the lifetime of the tube is estimated to be between 200-300 hours at the normal operating levels.

Table 3: Saturation activities for ^{57}Ni , ^{24}Na and ^{56}Mn from the irradiation of nickel, aluminum and iron foils placed 12" from the head, on the centerline (operated at 150 kV, 2.5 mA)

<i>Nuclide</i>	<i>Ni-57</i>	<i>Na-24</i>	<i>Mn-56</i>
Reaction	Ni-58(n,2n)Ni-57	Al-27(n, α)Na-24	Fe-56(n,p)Mn-56
Foil Weight (gm)	0.2833	0.0418	0.1362
Peak (keV)	1377.62	1368.598	846.81
Counts	60	66	3114 2345
Decay Time (sec)	1079	2375	643 4256
Total Count Time (sec)	3600.69	3600.79	1842.96 1837.32
Peak Efficiency (%)	1.302	1.308	3.115
Saturation Activity (Bq/atm)	4.3250E-20 \pm 12.9%	1.0488E-19 \pm 12.31%	1.9258E-19 \pm 1.8% 1.9245E-19 \pm 2.1%

Table 4: Saturation activities for ^{57}Ni , ^{58}Co , ^{24}Na and ^{56}Mn from the irradiation of nickel, aluminum and iron foils placed on the generator head, on the centerline (operated at 150 kV, 2.5 mA)

<i>Nuclide</i>	<i>Ni-57</i>	<i>Co-58</i>	<i>Na-24</i>	<i>Mn-56</i>
Reaction	Ni-58(n,2n)Ni-57	Ni-58(n,p)Co-58	Al-27(n, α)Na-24	Fe-56(n,p)Mn-56
Foil Weight (gm)	0.2835	0.2835	0.0425	0.1378
Peak (keV)	1377.62	810.772	1368.598	846.81
Counts	12936 4299 4194 4103 4196	2690 2756 2752 2829 -	4232 4139 4158 4144 4175	178654 156053 136853 118545 103446
Decay Time (sec)	852 78945 80762 82580 84307	78945 80762 82580 84397 -	2282 2899 3516 4133 4750	550 2405 4257 6104 7946
Count Time (sec)	3610.95 1802.87 1802.82 1802.8 1802.78	2690 2756 2752 2829 -	603.23 602.57 602.23 602.05 601.97	1842.96 1837.32 1832.51 1828.37 1824.71
Peak Efficiency (%)	0.4764	0.8170	0.4797	0.3884
Saturation Activity (Bq/atm)	2.540E-17 \pm 0.88% 2.565E-17 \pm 1.53% 2.527E-17 \pm 1.54% 2.497E-17 \pm 1.56% 2.578E-17 \pm 1.54%	2.264E-16 \pm 1.93% 2.320E-16 \pm 1.90% 2.317E-16 \pm 1.91% 2.382E-16 \pm 1.88% -	1.041E-16 \pm 1.54% 1.028E-16 \pm 1.55% 1.041E-16 \pm 1.55% 1.046E-16 \pm 1.55% 1.063E-16 \pm 1.55%	8.788E-17 \pm 0.24% 8.842E-17 \pm 0.25% 8.926E-17 \pm 0.27% 8.894E-17 \pm 0.29% 8.922E-17 \pm 0.31%

Table 5: Average neutron energy on centerline for the MF-Physics A-711 Neutron Generator
(operated at 150 kV, 2.5 mA)

Reaction Ratio	Al-27(n, α)Na-24/ Ni-58(n,2n)Ni-57	Ni-58(n,p)Co-58/ Ni-58(n,2n)Ni-57	Fe-56(n,p)Mn-56/ Ni-58(n,2n)Ni-57
12" Data			
Saturation Activity Ratio	2.425 \pm 17.84%	-	4.474 \pm 12.92%
Average Neutron Energy (MeV)	15.132 \pm 2.64%	-	14.141 \pm 0.41%
Near Head Data			
Saturation Activity Ratio	4.107 \pm 1.04%	9.130201 \pm 1.23%	3.491 \pm 0.78%
Average Neutron Energy (MeV)	14.302 \pm 0.18%	14.531 \pm 1.15%	14.416 \pm 0.40%

Table 6: Average neutron flux on centerline for the MF-Physics A-711 Neutron Generator
(operated at 150 kV, 2.5 mA)

Reaction	Ni-58(n,2n)Ni-57	Ni-58(n,p)Co-58	Al-27(n, α)Na-24	Fe-56(n,p)Mn-56
12" Data				
Cross Section (barns)	0.031954	-	0.112523	0.108964
Flux (n \cdot cm ⁻² \cdot s ⁻¹)	1.35E+06 \pm 2.40%	-	9.32E+05 \pm 0.50%	1.78E+06 \pm 2.17%
Near Head Data				
Cross Section (barns)	0.031953693	0.3304235	0.116794727	0.111297737
Flux (n \cdot cm ⁻² \cdot s ⁻¹)	7.95E+08 \pm 2.40%	7.02E+08 \pm 18.6%	8.94E+08 \pm 0.50%	7.97E+08 \pm 2.1%



Nuclear Engineering Division

Argonne National Laboratory
9700 South Cass Avenue, Bldg. 308
Argonne, IL 60439-4825

www.anl.gov



A U.S. Department of Energy laboratory
managed by The University of Chicago